

## INFRARED DEVICES AND TECHNIQUES (REVISION)

**A. Rogalski<sup>1</sup>, K. Chrzanowski<sup>2</sup>**

*1) Institute of Applied Physics, Military University of Technology, 2 Kaliskiego Str., 00-908 Warsaw, Poland*

*2) Institute of Optoelectronics, Military University of Technology, 2 Kaliskiego Str., 00-908 Warsaw, Poland*

### Abstract

In 2002 was published our review paper “Infrared devices and techniques” (*Opto-Electronics Review*, **10**(2), pp. 111-136). The present paper up-date previous edition – it content has been revised and much of materials have been reorganized.

The main objective of this paper is to produce an applications-oriented review covering infrared techniques and devices. At the beginning infrared systems fundamentals are presented with emphasis on thermal emission, scene radiation and contrast, cooling techniques, and optics. Special attention is focused on night vision and thermal imaging concepts. Next section concentrates shortly on selected infrared systems and is arranged in order to increase complexity; from image intensifier systems, thermal imaging systems, to space-based systems. In this section are also described active and passive smart weapon seekers. Finally, other important infrared techniques and devices are shortly described, among them being: non-contact thermometers, radiometers, LIDAR, and infrared gas sensors.

Keywords: thermal emission, radiation contrast, infrared bands, cooling technologies, infrared optical materials, night-vision systems, thermal imaging systems, image intensifier systems, focal plane arrays, space-based systems, smart weapon seekers, nocontact thermometers, radiometers, lidars, infrared gas sensors.

© 2014 Polish Academy of Sciences. All rights reserved

## 1. Introduction

Looking back over the past 1000 years, we notice that infrared (IR) radiation itself was unknown until more than 200 years ago (on February 15<sup>th</sup> 1800) when Herschel’s experiment with a thermometer was first reported. He built a crude monochromator that used a thermometer as a detector so that he could measure the distribution of energy in sunlight [1]. Following the works of Kirchhoff, Stefan, Boltzmann, Wien and Rayleigh, Max Planck culminated the effort with the well-known Planck’s law.

Traditionally, IR technologies are connected with controlling functions and night-vision problems with earlier applications connected simply with detection of IR radiation, and later by forming IR images from temperature and emissivity differences (systems for recognition and surveillance, tank sight systems, anti-tank missiles, air – air missiles). The years during World War II saw the origins of modern IR techniques. Recent success in applying IR technology to remote sensing problems has been made possible by the successful development of high-performance IR detectors over five decades. Most of the funding has been provided to fulfil military needs, but peaceful applications have increased continuously, especially in the last decade of the 20th century. These include medical, industry, earth resources and energy conservation applications. Medical applications include thermography, in which IR scans of the body detect cancers or other traumas, which raise the body surface temperature. Earth resource determinations are done by using IR images from satellites in

conjunction with field observation for calibration (in this manner, e.g. the area and content of fields and forests can be determined). In some cases, even the state of health of a crop can be determined from space. Energy conservation in homes and industry has been aided by the use of IR scans to determine the points of maximum heat loss. Demands to use these technologies are quickly growing due to their effective applications, e.g. in global monitoring of environmental pollution and climate changes, long time prognoses of agriculture crop yield, chemical process monitoring, Fourier transform IR spectrometry, IR astronomy, car driving, IR imaging in medical diagnostics and others.

The infrared range covers all electromagnetic radiation longer than the visible, but shorter than millimetre waves. Many proposals of IR range division have been published. The division shown below (table 1) is used by the military community and is based on the limits of spectral bands of commonly used IR detectors. Wavelength of 1  $\mu\text{m}$  is a sensitivity limit of popular Si detectors. Similarly, wavelength of 3  $\mu\text{m}$  is a long wavelength sensitivity of PbS and InGaAs detectors; wavelength of 6  $\mu\text{m}$  is a sensitivity limit of InSb, PbSe, PtSi detectors and HgCdTe detectors optimized for the 3–5  $\mu\text{m}$  atmospheric window; and finally wavelength of 15  $\mu\text{m}$  is a long wavelength sensitivity limit of HgCdTe detectors optimized for the 8–14  $\mu\text{m}$  atmospheric window.

Table 1. Division of infrared radiation.

Region (abbreviation)	Wavelength range ( $\mu\text{m}$ )
Near infrared (NIR)	0.78–1
Short wavelength IR (SWIR)	1–3
Medium wavelength IR (MWIR)	3–6
Long wavelength IR (LWIR)	6–15
Very long wavelength IR (VLWIR)	15–30
Far infrared (FIR)	30–100
Submillimetre (SubMM)	100–1000

## 2. Infrared system fundamentals

### 2.1 Thermal emission

All objects are composed of continually vibrating atoms, with higher energy atoms vibrating more frequently. The vibration of all charged particles, including these atoms, generates electromagnetic waves. The higher the temperature of an object, the faster the vibration, and thus the higher the spectral radiant energy. As a result, all objects are continually emitting radiation at a rate with a wavelength distribution that depends upon the temperature of the object and its spectral emissivity,  $\varepsilon(\lambda)$ .

Radiant emission is usually treated in terms of the concept of a blackbody [2]. A blackbody is an object that absorbs all incident radiation and conversely, according to the Kirchhoff law, is a perfect radiator. The energy emitted by a blackbody is the maximum theoretically possible for a given temperature. The radiative power (or number of photons emitted) and its wavelength distribution are given by the Planck radiation law:

$$W(\lambda, T) = \frac{2\pi hc^2}{\lambda^5} \left[ \exp\left(\frac{hc}{\lambda kT}\right) - 1 \right]^{-1}, \quad \text{W cm}^{-2} \mu\text{m}^{-1} \quad (1)$$

$$P(\lambda, T) = \frac{2\pi c}{\lambda^4} \left[ \exp\left(\frac{hc}{\lambda kT}\right) - 1 \right]^{-1}, \quad \text{photons s}^{-1} \text{cm}^{-2} \mu\text{m}^{-1} \quad (2)$$

where  $\lambda$  is the wavelength,  $T$  is the temperature,  $h$  is the Planck's constant,  $c$  is the velocity of light and  $k$  is the Boltzmann's constant.

Figure 1 shows a plot of these curves for a number of blackbody temperatures. As the temperature increases, the amount of energy emitted at any wavelength increases too, and the wavelength of peak emission decreases. The latter is given by the Wien displacement law:

$$\lambda_{mw}T = 2898 \mu\text{m K}, \quad \text{for maximum watts,}$$

$$\lambda_{mp}T = 3670 \mu\text{m K}, \quad \text{for maximum photons.}$$

The loci of these maxima are shown in figure 1. Note that for an object at the ambient temperature of 290 K,  $\lambda_{mw}$  and  $\lambda_{mp}$  occur at 10.0 and 12.7  $\mu\text{m}$ , respectively. We need detectors operating near 10  $\mu\text{m}$  if we expect to 'see' room temperature objects such as people, trees and trucks without the aid of reflected light. For hotter objects such as engines, the maximum emission occurs at shorter wavelengths. Thus, the waveband 2–15  $\mu\text{m}$  in infrared or thermal region of the electromagnetic spectrum contains the maximum radiative emission for thermal imaging purposes.

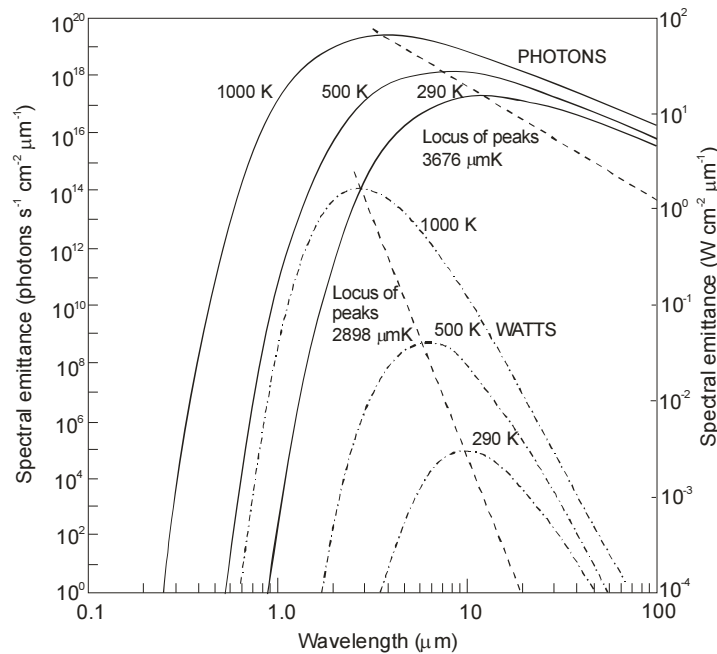


Fig. 1. Planck's law for spectral emittance.

## 2.2 Atmospheric transmission

Most of the above mentioned applications require transmission through air, but the radiation is attenuated by the processes of scattering and absorption. Scattering causes a change in the direction of a radiation beam; it is caused by absorption and subsequent reradiation of energy by suspended particles.

For larger particles, scattering is independent of wavelength. However, for small particles, compared with the wavelength of the radiation, the process is known as Rayleigh scattering and exhibits a  $\lambda^{-4}$  dependence. Therefore, scattering by gas molecules is negligibly small for wavelengths longer than 2  $\mu\text{m}$ . Also smoke and light mist particles are usually small with respect to IR wavelengths, and IR radiation can therefore penetrate further through smoke and mists than visible radiation. However, rain, fog particles and aerosols are larger and consequently scatter IR and visible radiation to a similar degree.

Figure 2 is a plot of the transmission through 6000 ft of air as a function of wavelength. Specific absorption bands of water, carbon dioxide and oxygen molecules that restrict atmospheric transmission to two windows at 3–5 and 8–14 μm, are indicated. Ozone, nitrous oxide, carbon monoxide and methane are less important IR absorbing constituents of the atmosphere.

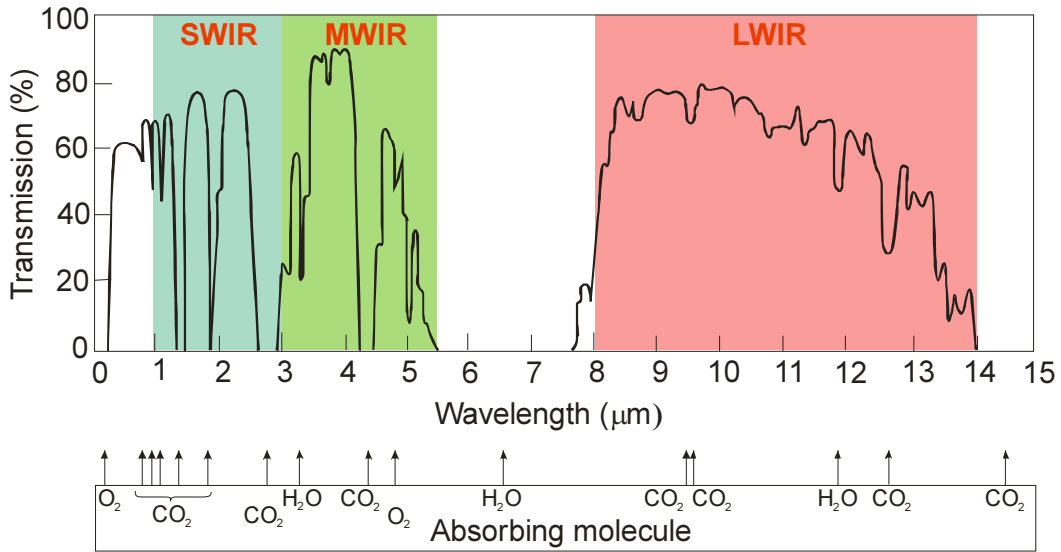


Fig. 2. Transmission of the atmosphere for a 6000 ft horizontal path at sea level containing 17 mm of precipitate water. Reproduced from [3].

### 2.3 Scene radiation and contrast

The total radiation received from any object is the sum of the emitted, reflected and transmitted radiation. Objects that are not blackbodies emit only the fraction  $\epsilon(\lambda)$  of blackbody radiation, and the remaining fraction,  $1 - \epsilon(\lambda)$ , is either transmitted or, for opaque objects, reflected. When the scene is composed of objects and backgrounds of similar temperatures, reflected radiation tends to reduce the available contrast. However, reflections of hotter or colder objects have a significant effect on the appearance of a thermal scene. The powers of 290 K blackbody emission and ground-level solar radiation in MWIR and LWIR bands are given in table 2. We can see that while reflected sunlight has a negligible effect on 8–14 μm imaging, it is important in the 3–5 μm band.

Table 2. Power available in each MWIR and LWIR imaging band.

IR region (μm) $\alpha$	Ground-level solar radiation (W m <sup>-2</sup> ) $\alpha$	Emission from 290 K blackbody (W m <sup>-2</sup> ) $\alpha$
3–5 $\alpha$	24 $\alpha$	4.1 $\alpha$
8–13 $\alpha$	1.5 $\alpha$	127 $\alpha$

A thermal image arises from temperature variations or differences in emissivity within a scene. The thermal contrast is one of the important parameters for IR imaging devices. It is the ratio of the derivative of spectral radiant exitance to the spectral radiant exitance

$$C = \frac{\partial W / \partial T}{W} \tag{3}$$

Figure 3 is a plot of  $C$  for several MWIR subbands and the 8–12- $\mu\text{m}$  LWIR spectral band. The contrast in a thermal image is small when compared with a visible image contrast due to differences in reflectivity. We can notice that the contrast in the MWIR bands at 300 K is 3.5–4 percent compared to 1.6 percent for the LWIR band. Thus, while the LWIR band may have higher sensitivity for ambient temperature objects, the MWIR band has greater contrast.

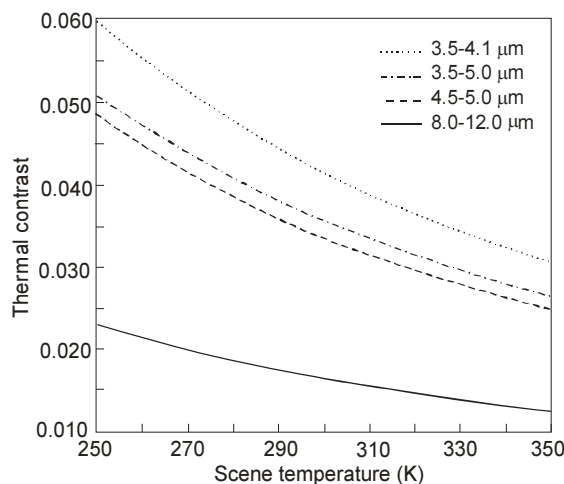


Fig. 3. Spectral photon contrast in the MWIR and LWIR bands.

#### 2.4 Choice of IR band

The SWIR wavelength band offers unique imaging advantages over visible and thermal bands. Like visible cameras, the images are primarily created by reflected broadband light sources, so SWIR images are easier for viewers to understand. Most materials used to make windows, lenses and coatings for visible cameras are readily useable for SWIR cameras, preventing cost increase. Ordinary glass transmits radiation to about 2.5  $\mu\text{m}$ . SWIR cameras can image many of the same light sources, such as Yag laser wavelengths. Thus, with safety concerns shifting laser operations to the "eye-safe" wavelengths where beams will not focus on the retina (beyond 1.4  $\mu\text{m}$ ), SWIR cameras are in a unique position to replace visible cameras for many tasks. Due to the reduced Rayleigh scatter of light at longer wavelengths, particulates in the air, such as dust or fog, SWIR cameras can see through haze better than visible cameras.

In general, the 8–14  $\mu\text{m}$  band is preferred for high performance thermal imaging because of its higher sensitivity to ambient temperature objects and its better transmission through mist and smoke. However, the 3–5  $\mu\text{m}$  band may be more appropriate for hotter objects, or if sensitivity is less important than contrast. Also additional differences occur, e.g. the advantage of the MWIR band is the smaller diameter of the optics required to obtain a certain resolution and the fact that some detectors may operate at higher temperatures (thermoelectric cooling) than is usual in the LWIR band where cryogenic cooling is required (about 77 K).

Summarizing, MWIR and LWIR  $\mu\text{m}$  spectral bands differ substantially with respect to background flux, scene characteristics, temperature contrast and atmospheric transmission under diverse weather conditions. Factors that favour MWIR applications are: higher contrast, superior clear weather performance (favourable weather conditions, e.g. in most countries of Asia and Africa), higher transmittivity in high humidity and higher resolution due to  $\sim 3\times$  smaller optical diffraction. Factors that favour LWIR applications are: better performance in fog and dust conditions, as well as winter haze (typical weather conditions, e.g. in West Europe, North USA, Canada), higher immunity to atmospheric turbulence and reduced sensitivity to solar glints and fire flares. The possibility of achieving a higher signal-to-noise (S/N) ratio due to greater radiance levels in LWIR spectral range is not persuasive because the

background photon fluxes are higher to the same extent, and also because of readout limitation possibilities. Theoretically, in staring arrays charge can be integrated for the full frame time, but because of restrictions in the charge-handling capacity of the readout cells, it is much less compared to the frame time, especially for LWIR detectors for which background photon flux exceeds the useful signals by orders of magnitude.

### 2.5 Detectors

The figure of merit used for detectors is detectivity. It has been found in many instances that this parameter varies inversely with the square root of both the detector's sensitive area,  $A$ , and the electrical bandwidth,  $\Delta f$ . In order to simplify the comparison of different detectors, the following definition has been introduced [4]

$$D^* = \frac{(A\Delta f)^{1/2}}{\Phi_e} (\text{SNR}), \quad (4)$$

where  $\Phi_e$  is the spectral radiant incident power.  $D^*$  is defined as the rms signal-to-noise ratio (SNR) in a 1 Hz bandwidth per unit rms incident radiation power per square root of detector area.  $D^*$  is expressed in  $\text{cm Hz}^{1/2} \text{W}^{-1}$ , which is recently called 'Jones'. Spectral detectivity curves for a number of commercially available IR detectors are shown in figure 4. Interest has centred mainly on the wavelengths of the two atmospheric windows 3–5 and 8–14  $\mu\text{m}$ , though in recent years there has been increasing interest in longer wavelengths stimulated by space applications.

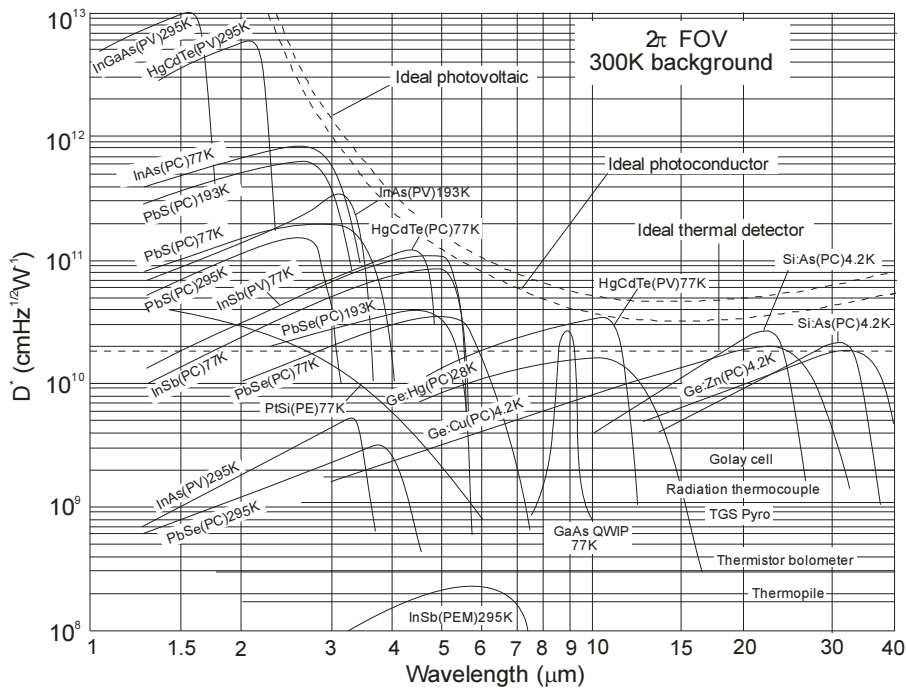


Fig. 4. Comparison of the  $D^*$  of various commercially available infrared detectors when operated at the indicated temperature. The chopping frequency is 1000 Hz for all detectors except the thermopile (10 Hz), thermocouple (10 Hz), thermistor bolometer (10 Hz), Golay cell (10 Hz) and pyroelectric detector (10 Hz). Each detector is assumed to view a hemispherical surround at a temperature of 300 K. Theoretical curves for the background-limited  $D^*$  for ideal photovoltaic and photoconductive detectors and thermal detectors are also shown.

Progress in IR detector technology is connected mainly to semiconductor IR detectors, which are included in the class of photon detectors. In this class, radiation is absorbed within the material by interaction with electrons. The observed electrical output signal results from

the changed electronic energy distribution. The photon detectors show a selective wavelength dependence of the response per unit incident radiation power. They exhibit both perfect signal-to-noise performance and a very fast response. But to achieve this, the photon detectors require cryogenic cooling. Cooling requirements are the main obstacle to the more widespread use of IR systems based on semiconductor photodetectors making them bulky, heavy, expensive and inconvenient to use. Depending on the nature of interaction, the class of photon detectors is further sub-divided into different types, the most important being: intrinsic detectors (HgCdTe, InGaAs, InSb, PbS, PbSe), extrinsic detectors (Si:As, Si:Ga), photoemissive (metal silicide Schottky barriers) detectors, quantum well detectors (GaAs/AlGaAs QWIPs), type-II superlattice III-V photodiodes and nBn barrier detectors.

The second class of IR detectors is composed of thermal detectors. In a thermal detector, the incident radiation is absorbed to change the temperature of material, and the resultant change in some physical properties is used to generate an electrical output. The detector element is suspended on lags, which are connected to the heat sink. Thermal effects are generally wavelength independent; the signal depends upon the radiant power (or its rate of change) but not upon its spectral content. In pyroelectric detectors, a change in the internal spontaneous polarization is measured, whereas in the case of bolometers a change in the electrical resistance is measured. In contrast to photon detectors, thermal detectors typically operate at room temperature. They are usually characterized by modest sensitivity and slow response but they are cheap and easy to use. The greatest utility in IR technology has been found by bolometers, pyroelectric detectors and thermopiles. Typical values of detectivities of thermal detectors at 10 Hz change in the range between  $10^8$  and  $10^9$  cm Hz<sup>1/2</sup> W<sup>-1</sup>.

Up until the nineties of the 20th century, thermal detectors were considerably less exploited in commercial and military systems in comparison with photon detectors. The reason for this disparity is that thermal detectors are popularly believed to be rather slow and insensitive compared to photon detectors. As a result, the worldwide effort to develop thermal detectors was extremely small relative to that of photon detectors. In the last two decades, however, it has been shown that extremely good imagery can be obtained from large thermal detector arrays operating uncooled at TV frame rates. The speed of thermal detectors is quite adequate for non-scanned imagers with two-dimensional (2D) detectors. The moderate sensitivity of thermal detectors can be compensated by a large number of elements in 2D electronically scanned arrays. With large arrays of thermal detectors the best values of noise equivalent difference temperature (*NEDT*), below 0.1 K, could be reached because effective noise bandwidths less than 100 Hz can be achieved.

Initially developed for the military market by US defence companies, IR uncooled cameras are now widely used in many commercial applications. Currently, the microbolometer detectors are produced in larger volumes than all other IR array technologies together. In large volume production for automobile drivers, the cost of uncooled imaging systems is below \$1000. The global infrared market value was estimated to be nearly \$321.4 million in 2013. It is expected to reach \$704.8 million by 2020, at a CAGR (*Compound Annual Growth Rate*) of 11.9% from 2014–2020 [5].

## 2.6 Cooling

The signal output of a photon detector is so small that at ordinary temperatures it is swamped by the thermal noise due to random generation and recombination of carriers in the semiconductor. In order to reduce the thermal generation of carriers and minimize noise, photon detectors must be cooled and must therefore be encapsulated. The method of cooling varies according to the operating temperature and the system logistical requirements.

The two technologies currently available for addressing the cooling requirements of IR and visible detectors are closed cycle refrigerators and thermoelectric coolers. Closed cycle refrigerators can achieve the cryogenic temperatures required for cooled IR sensors, while

thermoelectric coolers are generally the preferred approach to temperature control for uncooled visible and IR sensors. The major difference between the thermoelectric and mechanical cryocoolers is the nature of the working fluid. A thermoelectric cooler is a solid-state device that uses charge carriers (electrons or holes) as a working fluid, whereas mechanical cryocoolers use a gas such as helium as the working fluid. The selection of a cooler for a specific application depends on cooling capacity, operating temperature, procurement, cost and maintenance, and servicing requirements. A survey of currently operating cryogenic systems for commercial, military, and space applications is summarized in figure 5. Table 3 presents advantages and disadvantages of different cryocoolers for space applications.

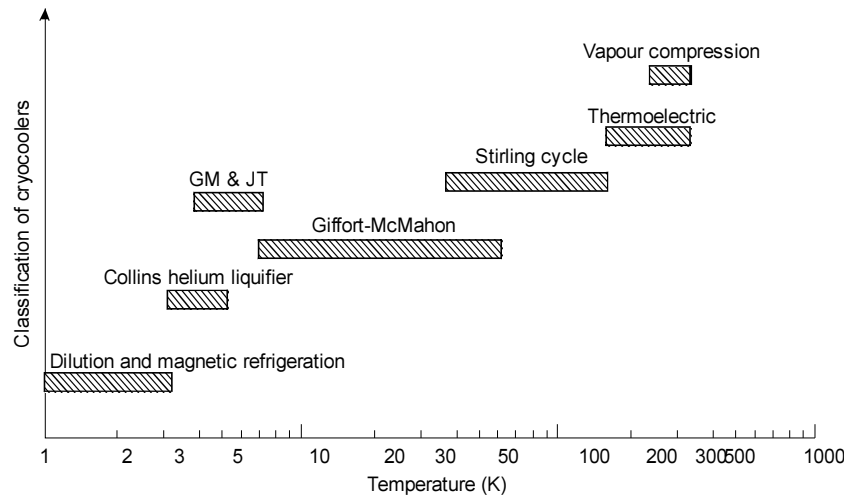


Fig. 5. Temperature ranges for commercial refrigerators.

Table 3. Cryocoolers for space applications.

Cooler	Typical temperature	Typical heat lift	Advantages	Disadvantages
Radiator	80 K	0.5 W	Reliable, low vibration, long lifetime	Complicates orbit
Stirling - 1 stage	80 K	0.8 W	Efficient, heritage	Vibrations
Stirling - 2 stage	20 K	0.06 W	Intermediate temp	Under development
Pulse tube	80 K	0.8 W	Lower vibrations, efficiency comparable to Stirling	Difficulties in scaling down to small sizes while maintaining high efficiency, larger diameter cold finger
Joule-Thompson	4 K	0.01 W	Low vibrations	Requires hybrid design
Sorption	10 K	0.1 W	Low vibrations	Low efficiency, under development
Brayton	65 K	8 W	High capacity	Complex
ADR	0.05 K	0.01 mW	Only way to reach these temps.	Large magnetic field
Peltier	170 K	1 W	Lightweight	High temp, low efficiency

Most 8–14- $\mu\text{m}$  detectors operate at approximately 77 K and can be cooled by liquid nitrogen. Cryogenic liquid pour-filled dewars are frequently used for detector cooling in laboratories. They are rather bulky and need to be refilled with liquid nitrogen every few hours. For many applications, especially in the field  $\text{LN}_2$ , pour-filled dewars are impractical, so many manufacturers are turning to alternative coolers that do not require cryogenic liquids or solids. It is more convenient to use Stirling and a Joule-Thompson minicoolers (see figure 6).



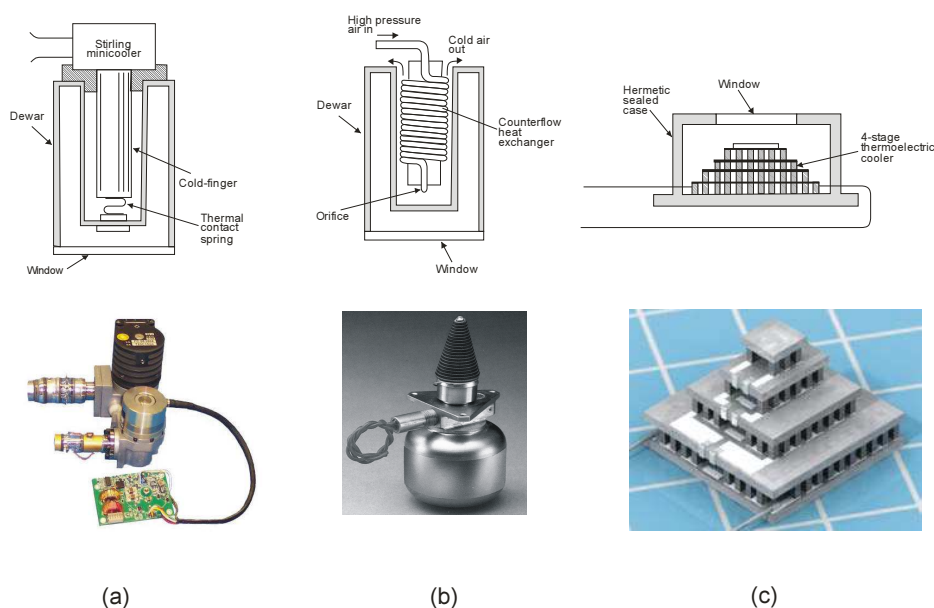


Fig. 6. Three ways of cooling IR detectors: (a) Stirling-cycle engine, (b) Joule-Thompson cooler, and (c) four-stage thermoelectric cooler.

Stirling coolers function by causing a working gas to undergo a Stirling cycle which consists of two constant volume processes and two isothermal processes. Devices consist of a compressor pump and a displacer unit with a regenerative heat exchanger, known as a regenerator. Stirling engines require several minutes of cool-down time; the working fluid is helium. The development of two-stage devices extends the lower temperature range from 60–80 to 15–30 K.

Both Joule-Thompson and engine-cooled detectors are housed in precision-bore dewars into which the cooling device is inserted (see figure 6). The detector, mounted in the vacuum space at the end of the inner wall of the dewar and surrounded by a cooled radiation shield compatible with the convergence angle of the optical system, looks out through an IR window. In some dewars, the electrical leads to detector elements are embedded in the inner wall of the dewar to protect them from damage due to vibration. After 3000 to 5000 h of operation, the Stirling cooler requires factory service to maintain performance. Because the dewar and cooler is one integrated detector assembly (or IDA) unit, the entire unit must be serviced together.

Split Stirling coolers are also fabricated. The detector is mounted on the dewar bore, and the cold finger of the cooler is thermally connected to the dewar by a bellows. A fan is necessary to dissipate the heat. The cooler can be easily removed from the detector/dewar for replacement.

The moving displacer in Stirling cryocoolers has several disadvantages. It is a source of vibration, has a limited lifetime, and contributes to axial heat conduction as well as to a shuttle heat loss. Pulse tube coolers are similar to Stirling coolers. However, their thermodynamic processes are quite different. The proper gas motion in phase with the pressure is achieved by the use of an orifice, along with a reservoir volume to store the gas during a half cycle. The reservoir volume is large enough to make negligible pressure oscillation occur in it during the oscillating flow. The oscillating flow through the orifice separates the heating and cooling effects just as the displacer does for the Stirling refrigerator.

Since there are no moving parts at the cold-end, reliability is theoretically higher than Stirling cycle machines. Efficiencies approaching Stirling cycle coolers can be achieved and several recent missions have demonstrated their usefulness in space.

The design of Joule-Thompson (J-T) coolers is based on the fact that as a high-pressure gas expands upon leaving a throttle valve, it cools and liquefies (leading to isenthalpic cooling). The coolers require a high-pressure gas supply from bottles and compressors. Although this is an irreversible process, with correspondingly low efficiency, Joule-Thompson coolers are simple, reliable, and have low electrical and mechanical noise levels.

Using compressed air, temperatures amounting to 80 K can be achieved in one or two minutes. The gas used must be purified to remove water vapour and carbon dioxide that could freeze and block the throttle valve. Specially designed Joule-Thompson coolers using argon are suitable for ultrafast cool-down (a few second cooling time). Recent advances in J-T cryocoolers have been associated with the use of mixed-gases as the working fluid rather than pure gases.

Thermoelectric (TE) cooling of detectors is simpler and less costly than closed-cycle cooling. Thermoelectric coolers work by exploiting the Peltier effect that refers to the creation of heat flux at the junction of two dissimilar conductors in the presence of current flow.

Commercially available coolers do not go beyond 6 stages. They are based on alloys of bismuth telluride and antimony telluride materials. Detectors are usually mounted in a hermetic encapsulation with a base designed to make good contact with a heat sink. TE coolers can achieve temperatures to  $\approx 200$  K, have about 20-year operating life, are small and rugged, and have low input power ( $< 1$  W for a 2-stage device and  $< 3$  W for a 3-stage device). Their main disadvantage is low efficiency (see table 3).

The TE coolers used for IR FPA operation include 1-stage (TE1, down to  $-20^{\circ}\text{C}$  or 253 K), 2-stage (TE2, down to  $-40^{\circ}\text{C}$  or 233 K), 3-stage (TE3, down to  $-65^{\circ}\text{C}$  or 208 K), and 4-stage (TE4, down to  $-80^{\circ}\text{C}$  or 193 K). Peltier coolers are also the preferred approach to temperature control at the required level, e.g., for uncooled visible and IR sensors.

## 2.7 IR optics

The optical block in an IR system creates an image of observed objects in the plane of the detector (detectors). In the case of a scanning imager, the optical scanning system creates an image with the number of pixels much greater than the number of elements of the detector. In addition, optical elements like windows, domes and filters can be used to protect the system from the environment or to modify the detector spectral response.

There is no essential difference in design rules of optical objectives for visible and IR ranges. The designer of IR optics is only more limited because there are significantly fewer materials suitable for IR optical elements, in comparison with those for the visible range, particularly for wavelengths over  $2.5\ \mu\text{m}$ .

There are two types of IR optical element: reflective elements and refractive elements. As the names suggest, the role of reflective elements is to reflect incident radiation and the role of refractive elements is to refract and transmit incident radiation.

Mirrors used extensively inside IR systems (especially in scanners) are most often met as reflective elements that serve manifold functions in IR systems. Elsewhere they need a protective coating to prevent them from tarnishing. Spherical or aspherical mirrors are employed as imaging elements. Flat mirrors are widely used to fold optical paths, and reflective prisms are often used in scanning systems.

Four materials are most often used for mirror fabrication: optical crown glass, low-expansion borosilicate glass (LEBG), synthetic fused silica and Zerodur. Less popular in use are metallic substrates (beryllium, copper) and silicon carbide. Optical crown glass is typically applied in nonimaging systems. It has a relatively high thermal expansion coefficient and is employed when thermal stability is not a critical factor. LEBG, known by the Corning brand name Pyrex, is well suited for high quality front surface mirrors designed for low optical deformation under thermal shock. Synthetic fused silica has a very low thermal expansion coefficient.

Metallic coatings are typically used as reflective coatings of IR mirrors. There are four types of most often used metallic coating, namely bare aluminium, protected aluminium, silver and gold. They offer high reflectivity, over about 95%, in the 3–15  $\mu\text{m}$  spectral range. Bare aluminium has a very high reflectance value but oxidizes over time. Protected aluminium is a bare aluminium coating with a dielectric overcoat that arrests the oxidation process. Silver offers better reflectance in the near IR than aluminium and high reflectance across a broad spectrum. Gold is a widely used material and offers consistently very high reflectance (about 99%) in the 0.8–50  $\mu\text{m}$  range. However, gold is soft (it cannot be touched to remove dust) and is most often used in the laboratory.

Most glasses used to manufacture optical elements for visible and near infrared range transmit well light up to about 2.2  $\mu\text{m}$  and can be used for SWIR optics. Thermal imagers use almost exclusively two spectral bands: 3 to 5  $\mu\text{m}$  or 8–14  $\mu\text{m}$ . Therefore, materials typically considered for infrared optics are those suitable to transmit infrared radiation in spectral range from 2  $\mu\text{m}$  to 14  $\mu\text{m}$ .

The list of potential materials that could be used to manufacture infrared refractive optics is quite long: AMTIR-1 (Amorphous Material Transmitting Infrared Radiation), barium fluoride ( $\text{BaF}_2$ ), cadmium telluride ( $\text{CdTe}$ ), calcium fluoride ( $\text{CaF}_2$ ), cesium bromide ( $\text{CsBr}$ ), cesium iodide ( $\text{CsI}$ ), fused silica-IR grade, gallium arsenide ( $\text{GaAs}$ ), germanium ( $\text{Ge}$ ), lithium fluoride ( $\text{LiF}$ ), magnesium fluoride ( $\text{MgF}_2$ ), potassium bromide ( $\text{KBr}$ ), potassium chloride ( $\text{KCl}$ ), silicon ( $\text{Si}$ ), sodium chloride ( $\text{NaCl}$ ), thallium bromoiodide (KRS-5), zinc selenide ( $\text{ZnSe}$ ), zinc sulfide ( $\text{ZnS}$ ). However, only several most popular materials used to manufacture refractive optical objectives for thermal imagers will be discussed in the paper. Basic parameters of these materials are presented in table 4 and their IR transmission is shown in figure 7.

Table 4. Principal characteristics of some infrared materials (after Ref. 6).

Material	Waveband ( $\mu\text{m}$ )	$n_{4\mu\text{m}}$ , $n_{10\mu\text{m}}$	$dn/dT$ ( $10^{-6} \text{ K}^{-1}$ )	Density ( $\text{g/cm}^3$ )	Other characteristics
Ge	2–12	4.0245, 4.0031	424 (4 $\mu\text{m}$ ) 404 (10 $\mu\text{m}$ )	5.32	Brittle, semiconductor, diamond-turning capability, visibly opaque, hard
Chalcogenide glasses	3–12	2.5100, 2.4944	55 (10 $\mu\text{m}$ )	4.63	Amorphous IR glass, can be slumped to near-net shape
Si	1.2–7.0	3.4289 (4 $\mu\text{m}$ )	159 (5 $\mu\text{m}$ )	2.329	Brittle, semiconductor, diamond-turned with difficulty, visibly opaque, hard
GaAs	3–12	3.304, 3.274	150	5.32	Brittle, semiconductor, visibly opaque, hard
ZnS	3–13	2.251, 2.200	43 (4 $\mu\text{m}$ ) 41 (10 $\mu\text{m}$ )	4.08	Yellowish, moderate hardness and strength, can be diamond-turning, scatters short wavelengths
ZnSe	0.55–20	2.4324, 2.4053	63 (4 $\mu\text{m}$ ) 60 (10 $\mu\text{m}$ )	5.27	Yellow-orange, relatively soft and weak, diamond-turning capability, very low internal absorption and scatter
$\text{CaF}_2$	3–5	1.410	–8.1 (3.39 $\mu\text{m}$ )	3.18	Visibly clear, diamond-turning capability, mildly hygroscopic
Sapphire	3–5	1.677( $n_o$ ) 1.667( $n_e$ )	6 (o) 12 (e)	3.99	Very hard, difficult to polish due to crystal boundaries
BF7 (Glass)	0.35–2.3		3.4	2.51	Typical optical glass

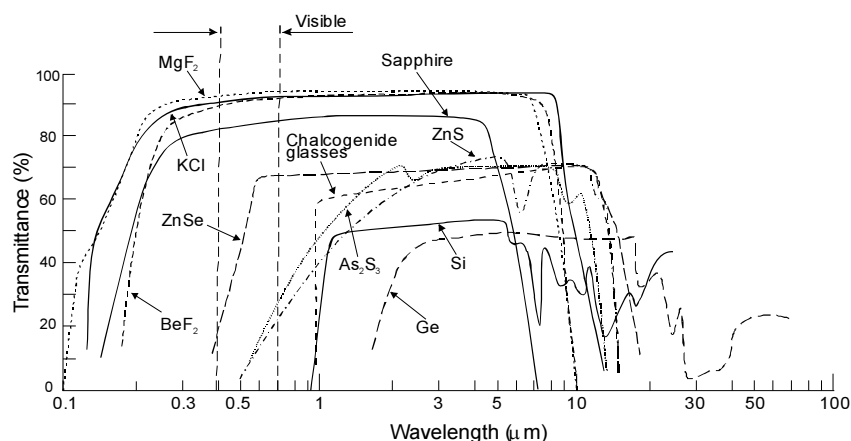


Fig. 7. Transmission range of infrared materials. Reproduced from [6].

Germanium is a silvery metallic-appearing solid of very high refractive index ( $> 4$ ) that enables design of high-resolution optical systems using a minimal number of germanium lenses. Its useful transmission range constitutes from 2 to about 15  $\mu\text{m}$ . It is quite brittle and difficult to cut but accepts a very good polish. Germanium is non-hygroscopic and non-toxic, has good thermal conductivity, excellent surface hardness, and good strength. Additionally, due to its very high refractive index, antireflection coatings are essential for any germanium transmitting optical system. Germanium has low dispersion and is unlikely to need colour correcting except in the highest-resolution systems. A significant disadvantage of germanium is the serious dependence of its refractive index on temperature, so germanium lenses may need to be athermalized. In spite of high material price and cost of antireflection coatings, germanium is a favourite choice of optical designers of high performance infrared objectives for thermal imagers.

Infrared chalcogenide classes offer good transmission from about 1  $\mu\text{m}$  to about 13  $\mu\text{m}$  (from SWIR to LWIR range). Physical properties such as low  $dn/dT$  and low dispersion enable optical designers to engineer colour-correcting optical systems without thermal defocusing. A moldable feature of these glasses allows a cost-effective manufacture of complex lens geometries in medium to large volumes. Moreover, these glasses can be also processed using conventional grinding and polishing techniques, single point diamond turning if higher performance is to be achieved. Due to these features infrared chalcogenide glasses have made a revolution in manufacturing of optics for thermal imagers during the last decades by enabling mass manufacturing of low cost, good optical performance optical objectives; and now these glasses compete with germanium as the most popular IR optical material. Most popular brands of infrared chalcogenide glasses are: AMTIR from Amorphous Materials Inc., GASIR® from Umicore Inc., and IRG glasses from Schott. It should be however noted that chalcogenide glasses are more difficult for fabrication of high accuracy lenses comparing to germanium.

Physical and chemical properties of silicon are very similar to the properties of germanium. It has a high refractive index ( $\approx 3.45$ ), is brittle, does not cleave, takes an excellent polish and has large  $dn/dT$ . Similarly to germanium, silicon optics must have antireflection coatings. Silicon offers two transmission ranges: 1–7 and 25–300  $\mu\text{m}$ . Only the first one is used in typical IR systems. The material is significantly cheaper than germanium, ZnSe and ZnS. It is used mostly for IR systems operating in the 3–5  $\mu\text{m}$  band. Due to its low density silicon is an ideal choice for MWIR objectives with weight constraints.

ZnSe is an optical material of optical properties mostly similar to germanium but of wider transmission range from about 0.55  $\mu\text{m}$  to about 20  $\mu\text{m}$ , and a refractive index of about 2.4. It is partially translucent in the visible and reddish in colour. Due to the relatively high refractive index, antireflection coatings are necessary. It has excellent chemical resistance and

is a popular material for lenses for both LWIR and MWIR objectives and for broadband infrared windows.

ZnS offers relatively good transmission in range from about 3  $\mu\text{m}$  to 13  $\mu\text{m}$ . It exhibits exceptional high fracture strength, high hardness, and high chemical resistance. Due to its high resistance to rain erosion and high-speed dust abrasion ZnS is popular for windows or external lenses in thermal imagers used in high speed airborne applications.

Ordinary glass does not transmit radiation beyond 2.5  $\mu\text{m}$  in the IR region. Fused silica is characterized by a very low thermal expansion coefficient that makes optical systems particularly useful in changing environmental conditions. It offers a transmission range from about 0.3 to 3  $\mu\text{m}$ . Because of low reflection losses due to the low refractive index ( $\approx 1.45$ ), antireflection coatings are not needed. However, an antireflection coating is recommended to avoid ghost images. Fused silica is more expensive than BK-7, but still significantly cheaper than Ge, ZnS and ZnSe, and is a popular material for lenses of IR systems with bands located below 3  $\mu\text{m}$ .

The alkali halides have excellent IR transmission; however, they are either soft or brittle and many of them are attacked by moisture, making them generally unsuitable for industrial applications. For more detailed discussion of the IR materials, see references [7,8].

## *2.8 Night-vision system concepts*

Night-vision systems can be divided into two categories: those depending upon the reception and processing of radiation reflected by an object and those which operate with radiation internally generated by an object. The latter systems are described in the subsection below. These devices gather existing ambient light (starlight, moonlight or infra-red light) through the front lens. This light, made up of photons, goes into a photocathode tube that changes the photons to electrons.

The human visual perception system is optimized to operate in daytime illumination conditions. The visual spectrum extends from about 420 to 700 nm and the region of greatest sensitivity is near the peak wavelength of sunlight at around 550 nm. However, at night fewer visible light photons are available and only large, high-contrast objects are visible. It appears that the photon rate in the region from 800 to 900 nm is five to seven times greater than in the visible region around 500 nm. Moreover, the reflectivity of various materials (e.g. green vegetation, because of its chlorophyll content) is higher between 800 and 900 nm than at 500 nm. It means that at night more light is available in the NIR than in the visual region and that against certain backgrounds more contrast is available.

The early concepts of image intensification were not basically different from those of today. However, the early devices suffered from two major deficiencies: poor photocathodes and poor coupling. Later development of both cathode and coupling technologies changed the image intensifier into a much more useful device. The concept of image intensification by cascading stages was suggested independently by a number of workers in the early 1930s.

A considerable improvement in night-vision capability can be achieved with night viewing equipment which consists of an objective lens, image intensifier and eyepiece (see figure 8). Improved visibility is obtained by gathering more light from the scene with an objective lens than an unaided eye; by use of a photocathode that has higher photosensitivity and broader spectral response than the eye; and by amplification of photo-events for visual sensation.

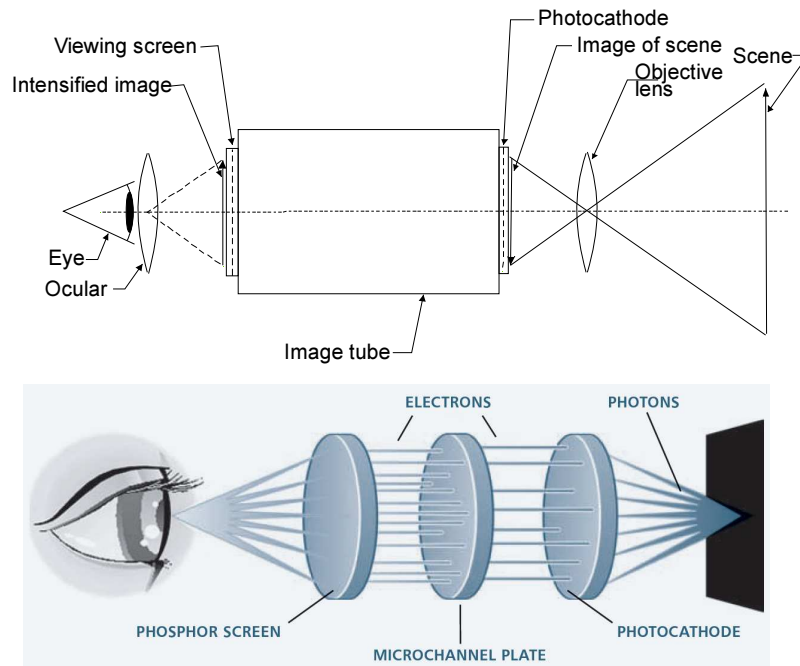


Fig. 8. Diagram of an image intensifier.

### 2.9 Thermal imaging system concepts

Thermal imaging is a technique for converting a scene's thermal radiation pattern (invisible to the human eye) into a visible image. Its usefulness is due to the following aspects:

- it is a totally passive technique and allows day and night operation;
- it is ideal for detection of hot or cold spots, or areas of different emissivities, within a scene;
- thermal radiation can penetrate smoke and mist more readily than visible radiation;
- it is a real-time, remote sensing technique.

The thermal image is a pictorial representation of temperature difference. Displayed on a scanned raster, the image resembles a television picture of the scene and can be computer processed to colour-code temperature ranges. Originally developed (in the 1960s) to extend the scope of night-vision systems, thermal imagers at first provided an alternative to image intensifiers. As the technology has matured, its range of application has expanded and now extends into the fields that have little or nothing to do with night vision (e.g. stress analysis, medical diagnostics). In most present-day thermal imagers, an optically focused image is scanned electronically across detectors (many elements or 2D array) the output of which is converted into a visual image. The optics, mode of scanning and signal processing electronics are closely interrelated. The number of picture points in the scene is governed by the nature of the detector (its performance) or the size of the detector array. The effective number of picture points or resolution elements in the scene is steadily increased.

Detectors are only a part of usable sensor systems. Military sensor systems include optics, coolers, pointing and tracking systems, electronics, communication, processing together with information-extraction sub-systems, and displays (see figure 9). Thus, the process of developing sensor system is significantly more challenging than fabricating a detector array.

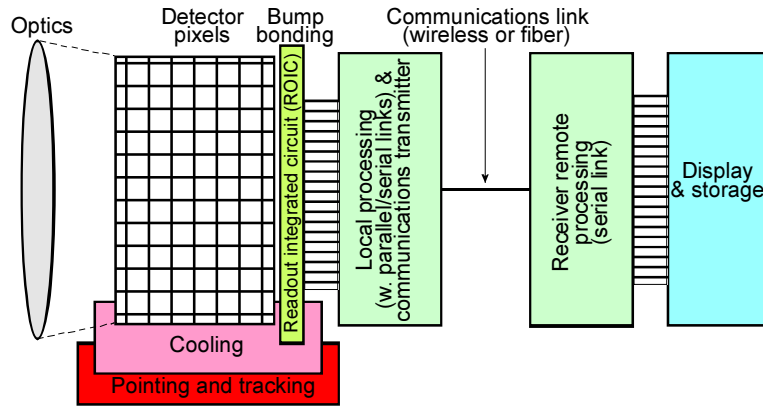


Fig. 9. Schematic representation of an imaging system showing important sub-systems.

Noise equivalent difference temperature (*NEDT*) is a figure of merit for thermal imagers, which is commonly reported. In spite of its widespread use in the infrared literature, it is applied to different systems, in different conditions, and with different meanings.

*NEDT* of a detector represents the temperature change, for incident radiation, that gives an output signal equal to the rms noise level. While normally thought of as a system parameter, detector *NEDT* and system *NEDT* are the same except for system losses. *NEDT* is defined

$$NEDT = \frac{V_n(\partial T/\partial Q)}{(\partial V_s/\partial Q)} = V_n \frac{\Delta T}{\Delta V_s}, \quad (5)$$

where  $V_n$  is the rms noise,  $Q$  is the spectral photon flux density (photons/cm<sup>2</sup>s) incident on a focal plane, and  $\Delta V_s$  is the signal measured for the temperature difference  $\Delta T$ .

It can be shown that *NEDT* is given by [9]:

$$NEDT = \frac{4f_{\#}^2(\Delta f)^{1/2}}{A^{1/2}t_{op}M^*}, \quad (6)$$

where  $f_{\#}$  is the f-number of the detector optics ( $f_{\#} = f/D$ ;  $f$  is the focal length and  $D$  the diameter of the lens),  $t_{op}$  the transmission of the optics and  $M^*$  the figure of merit that includes not only the detector performance  $D^*$  but also the spectral dependence of the emitted radiation,  $(\partial L/\partial T)_{\lambda}$ , and the atmospheric transmission  $t_{at}$ . It is given by the following equation:

$$M^* = \int_0^{\infty} \left( \frac{\partial L}{\partial T} \right)_{\lambda} t_{at\lambda} D_{\lambda}^* d\lambda. \quad (7)$$

Usually, the performance of MW and LWIR FPAs is limited by the readout circuits (by storage capacity of the ROIC). In this case [10]:

$$NEDT = (\tau C \eta \sqrt{N_w})^{-1}, \quad (8)$$

where  $N_w$  is the number of photogenerated carriers integrated for one integration time,  $t_{int}$

$$N_w = \eta A_d t_{int} Q_B. \quad (9)$$

According to the above formulas, the charge handling capacity of the readout, the integration time linked to the frame time, and dark current of the sensitive material become the major issues of IR FPAs. The *NEDT* is inversely proportional to the square root of the integrated charge, and therefore the greater the charge, the higher the performance. The well charge capacity is the maximum amount of the charge that can be stored in the storage

capacitor of each cell. The size of the unit cell is limited to the dimensions of the detector element in the array.

To receive best sensitivity (lowest *NEDT*), the spectral integral in Eq. (6) should be maximized. This can be obtained when the peak of the spectral responsivity and the peak of the exitance contrast coincide. However, the thermal imaging system may not satisfy these conditions because of other constrains, such as atmospheric/abscurant transmittance effects or available detector characteristics. Dependence on the square root of bandwidth is intuitive, since the root-mean-square (rms) noise is proportional to  $(\Delta f)^{1/2}$ . In addition, better *NEDT* result from lower *f*/#. A lower *f*/# number results in more flux captured by the detector, which increases SNR for a given level.

The dependence of *NEDT* on the detector area,  $A_d$ , is critical. The inverse-square-root dependence of *NEDT* on the detector area results as an effect of two terms: increasing of rms noise as the square root of the detector area and proportional increasing of the signal voltage to the area of detector. The net result is that  $NEDT \propto 1/(A_d)^{1/2}$ . While the thermal sensitivity of imager is better for larger detectors, the spatial resolution is poorer for larger detectors (pixels). Another parameter, the minimum resolvable difference temperature (*MRDT*), considering both thermal sensitivity and spatial resolution, is more appropriate for design (more information – see section 3.2).

The previous considerations are valid assuming that the temporal noise of the detector is the main source of noise. However, this assertion is not true to staring arrays, where the nonuniformity of the detectors response is a significant source of noise. This nonuniformity appears as a fixed pattern noise (spatial noise). It is defined in various ways in the literature, however, the most common definition is that it is the dark signal nonuniformity arising from an electronic source (i.e. other than thermal generation of the dark current); e.g. clock breakthrough or from offset variations in row, column or pixel amplifiers/switches. Thus, the estimation of IR sensor performance must include a treatment of spatial noise that occurs when FPA nonuniformities cannot be compensated correctly.

Mooney *et al.* [11] have given a comprehensive discussion on the origin of spatial noise. The total noise of a staring array is the composite of the temporal noise and the spatial noise. The spatial noise is the residual nonuniformity  $u$  after application of nonuniformity compensation, multiplied by the signal electrons  $N$ . Photon noise, equal to  $N^{1/2}$ , is the dominant temporal noise for the high IR background signals for which spatial noise is significant. Then, the total *NEDT* is

$$NEDT_{total} = \frac{(N + u^2 N^2)^{1/2}}{\partial N / \partial T} = \frac{(1/N + u^2)^{1/2}}{(1/N)(\partial N / \partial T)}, \quad (10)$$

where  $\partial N / \partial T$  is the signal change for a 1 K source temperature change. The denominator,  $(\partial N / \partial T) / N$ , is the fractional signal change for a 1 K source temperature change. This is the relative scene contrast.

The dependence of the total *NEDT* on detectivity for different residual nonuniformity is plotted in figure 10 for 300 K scene temperature and set of parameters shown insert the figure. When the detectivity is approaching a value above  $10^{10}$  cmHz<sup>1/2</sup>/W, the FPA performance is uniformity limited prior to correction and thus essentially independent of the detectivity. An improvement in nonuniformity from 0.1% to 0.01% after correction could lower the *NEDT* from 63 to 6.3 mK.



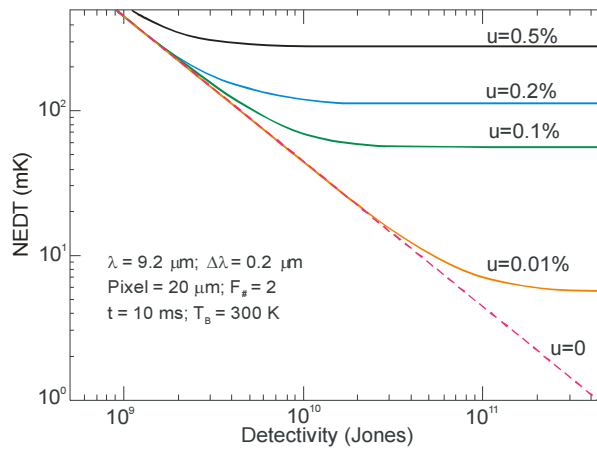


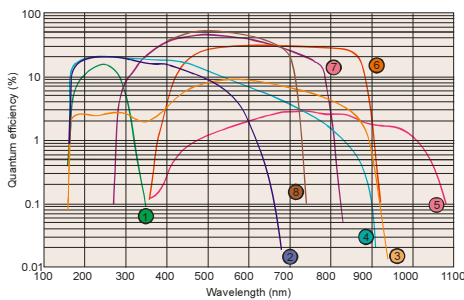
Fig. 10.  $NE\Delta T$  as a function of detectivity. The effects of nonuniformity are included for  $u = 0.01\%$ ,  $0.1\%$ ,  $0.2\%$  and  $0.5\%$ . Note that for  $D^* > 10^{10}$   $\text{cmHz}^{1/2}/\text{W}$ , detectivity is not the relevant figure of merit.

### 3. IR systems

This section briefly concentrates on selected IR systems and is arranged in the order of increasing complexity – from an image intensifier to space-base systems. A comprehensive compendium devoted to IR systems was copublished in 1993 by the Infrared Information Analysis Center (IRIA) and the International Society for Optical Engineering (SPIE) as *The Infrared and Electro-Optical Systems Handbook* (executive editors: Joseph S Accetta and David L Shumaker).

#### 3.1 Image intensifier systems

The concepts of image intensification (see figure 8) created in the early 1930s were not basically different from those of today. However, the early devices suffered from two major deficiencies: poor photocathodes and poor coupling. Later development of both cathode and coupling technologies changed the image intensifier into much more useful device [12]. Typical spectral sensitivity curves of various photocathodes charge with typical transmittance of window materials together with a list of important photocathodes are show in figure 11.



Suffix	Photocathode	Input window
1	CsTe	Synthetic silica
2	Bialkali	Synthetic silica
3	Enhanced multialkali	red Synthetic silica
4	Multialkali	Synthetic silica
5	InGaAs	Borosilicate glass
6	GaAs	Borosilicate glass
7	Enhanced red GaAsP	Borosilicate glass
8	GaAsP	Borosilicate glass

Fig. 11. Spectral sensitivity curves of various photocathodes. Reproduced from [13].

As is shown in figure 8, the image intensifier system is built from three main blocks: an optical objective, multichannel plate (MCP), and optical ocular. An MCP is a secondary electron multiplier consisting of an array of millions of very thin glass channels (of internal diameter  $\approx 10 \mu\text{m}$ , each capillary works as an independent electron multiplier) bundled in parallel and sliced in the form of a disc (see figure 12). Secondary electrons are accelerated by the voltage applied across the both ends of the MCP. This process is repeated many times along the channel wall and as a result, a great number of electrons are output from the MCP.

Furthermore, the electron flux can be reconverted into an optical image by using a phosphor coating as the rear electrode to provide electroluminescence; this combination provides an image intensifier.

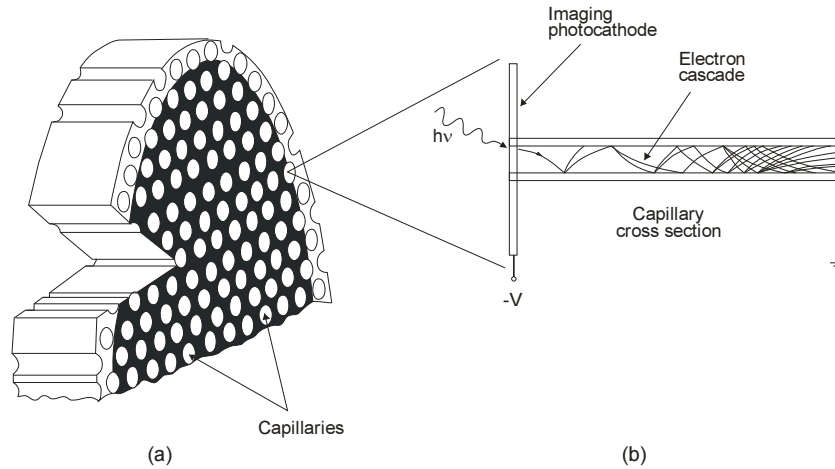






Fig. 12. Schematic presentation of microchannel plate: (a) cutway view and (b) a single capillary.

Image intensifiers are classed by generation (Gen) numbers. Gen0 refers to the technology of World War II, employing fragile, vacuum-enveloped photon detectors with poor sensitivity and little gain. Further evolution of image intensifier tubes is presented in table 5. Gen1 represents the technology of the early Vietnam era, the 1960s. In this era, the first passive systems, able to amplify ambient starlight, were introduced. Though sensitive, these devices were large and heavy. Gen1 devices used tri-alkali photocathodes to achieve gain of about 1000. By the early 1970s, the MCP amplifier was developed comprising more than two million microscopic conducting channels of hollow glass, each of about 10  $\mu\text{m}$  in diameter, fused into a disc-shaped array. Coupling the MCP with multi-alkali photocathodes, capable of emitting more electrons per incident photon, produced GenII. GenII devices boasted amplifications of 20 000 and operational lives to 4000 h. Interim improvements in bias voltage and construction methods produced the GenII<sup>+</sup> version. Substantial improvements in gain and bandwidth in the 1980s heralded the advent of GenIII. Gallium arsenide photocathodes and internal changes in the MCP design resulted in gains ranging from 30 000 to 50 000 and operating lives of 10 000 h.

Table 5. Image intensifier tubes – history and basic parameters. Reproduced from [12].

GenI	GenII	GenIII	GenIII Filmless
			
<ul style="list-style-type: none"> <li>• Vietnam War</li> <li>• SbCs i SbNa<sub>2</sub>KCs photocathodes (S10,S20)</li> <li>• electrostatic inversion</li> <li>• photosensitivity up to 200 <math>\mu\text{A}/\text{lm}</math></li> </ul>	<ul style="list-style-type: none"> <li>• 1970s</li> <li>• multialkali photocathodes (S25)</li> <li>• microchannel plate (MCP)</li> <li>• photosensitivity up to 700 <math>\mu\text{A}/\text{lm}</math></li> <li>• operational live to 4,000 h</li> </ul>	<ul style="list-style-type: none"> <li>• early 1980s</li> <li>• GaAs photocathodes</li> <li>• ion barrier to microchannel plate</li> <li>• photosensitivity up to 1,800 <math>\mu\text{A}/\text{lm}</math></li> <li>• operational live to 10,000 h</li> </ul>	<ul style="list-style-type: none"> <li>• late 1990s</li> <li>• multialkali photocathodes</li> <li>• "filmless" tube</li> <li>• photosensitivity up to 2,200 <math>\mu\text{A}/\text{lm}</math></li> <li>• operational time to 10,000 h</li> </ul>

Gen No	Photocathode material	Photocathode sensitivity [ $\mu\text{A}/\text{lm}$ ]	Design type	Luminance gain [ $\text{lm}/\text{lm}$ ]	Resolution [ $\text{lp}/\text{mm}$ ]	SNR
0	S1	< 60	inverter tube	< 200	20–60	–
I	S20	< 160	inverter tube	< 800	20–60	–
I+	S20	< 160	cascade inverter tube	< 20,000	20–30	5–8
II	S25	< 350	inverter MCP tube	< 50,000	24–43	12–17
II+	improved S25	< 700	proximity focus MCP tube	< 70,000	43–81	16–24
III	GaAs/GaAsP	< 1,600	proximity focus MCP tube with protecting film	< 70,000	36–64	18–25
III+ Thin film	GaAs/GaAsP	< 1,800	proximity focus MCP thin film tubes	< 70,000	57–71	24–28
III Filmless	GaAs/GaAsP	< 2,200	proximity focus MCP filmless tubes	< 80,000	57–71	24–31

Figure 13 shows the response of a typical Gen3 image intensifier superimposed on the night sky radiation spectrum [14]. This figure also shows the CIE photopic curve illustrating the spectral response of the human visual perception system, and the GenII response.

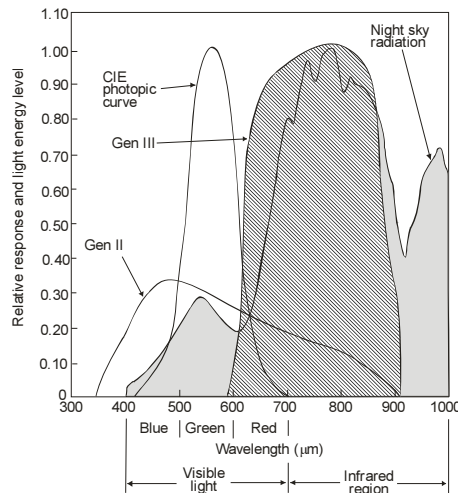


Fig. 13. Image intensifier tube spectral response curves. Reproduced from [14].

Many candidate technologies could form the basis of a GenIV, ranging from enhanced current designs to completely different approaches. Among them are devices with a new photocathode that extend spectral response to 1.6  $\mu\text{m}$  and the use of an amplifying mechanism other than MCPs. Other potentials include lightweight systems that fuse the outputs from image intensifiers and thermal imagers, as well as those that couple electron-bombarded CCD arrays—providing sensitivity in the NIR and MWIR regions—with miniature flat-panel displays. The first GenIV tubes demonstrated substantial increase in target detection range and resolution, particularly at extremely low light levels.

Various implementations of image intensifier tubes have been realized. Phosphor output image intensifiers were reviewed in depth by Csorba [15]. The image is focused onto a semitransparent photocathode and photoelectrons are emitted with a spatial intensity distribution which matches the focused image. In image intensifiers, the electrons are then accelerated towards a phosphor screen where they reproduce the original image with enhanced intensity. Three common forms of image tubes are shown in figure 14.

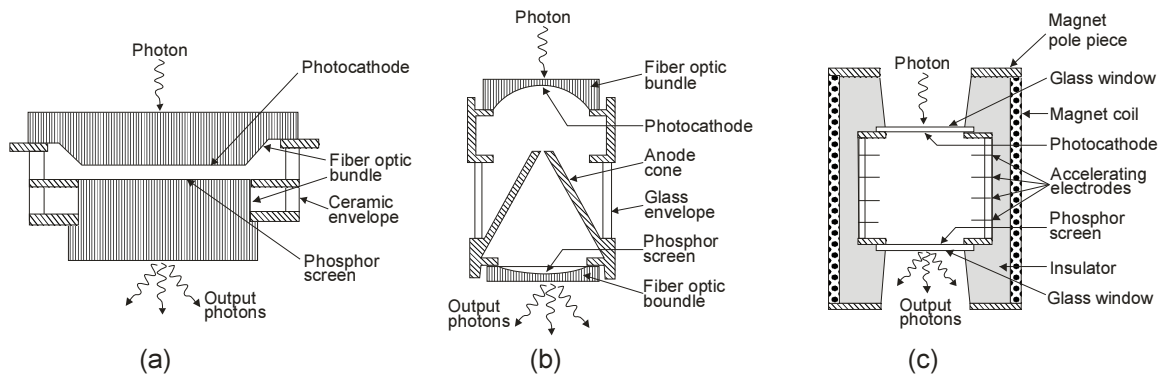


Fig. 14. Cross-sectional diagrams of a variety of image intensifier types: (a) proximity focused, (b) electronically focused and (c) magnetically focused. Reproduced from [15].

In a ‘proximity-focused’ tube, a high electric field (typically 5 kV), and a short distance between the photocathode and the screen, limit spreading of electrons to preserve an image. This form of tube is compact, the image is free from distortion and only a simple power supply is required. However, the resolution of such a tube is limited by the field strength at the photocathode and the resolution is highest when the distance between the cathode and the screen is small.

An electrostatically focused tube is based upon a system of concentric spheres (cathode and anode, typical bias voltage of 15 kV). In practice, the electrodes depart radically from the simple spherical concept. Additional electrodes can be introduced to provide focusing control and reduce the image distortion, while fibre-optic windows at input and output can be used to improve image quality and provide a better matching to objective and coupling optics. Power supplies are very simple and lightweight, that is why this type of tube is widely used in portable applications.

A magnetically focused system gives very high-resolution imagers with little or no distortion. The focusing coil, however, is usually heavy and power consuming. For the best picture quality, the power suppliers for both tube and coil must be stable. This type of tube is used in applications where resolution and low distortion are vital and weight and power consumption do not create unacceptable problems.

Image intensifiers were primarily developed for nighttime viewing and surveillance under moonlight or starlight. At present, image intensifier applications have spread from nighttime viewing to various fields including industrial product inspection and scientific research, especially when used with CCD cameras – so called intensified CCD or ICCD [see figure 15(a)]. Gate operation models are also useful for observation and motion analysis of high-speed phenomena (high-speed moving objects, fluorescence lifetime, bioluminescence and chemiluminescence images). Figure 15(b) shows an example of Gen III night vision goggle.

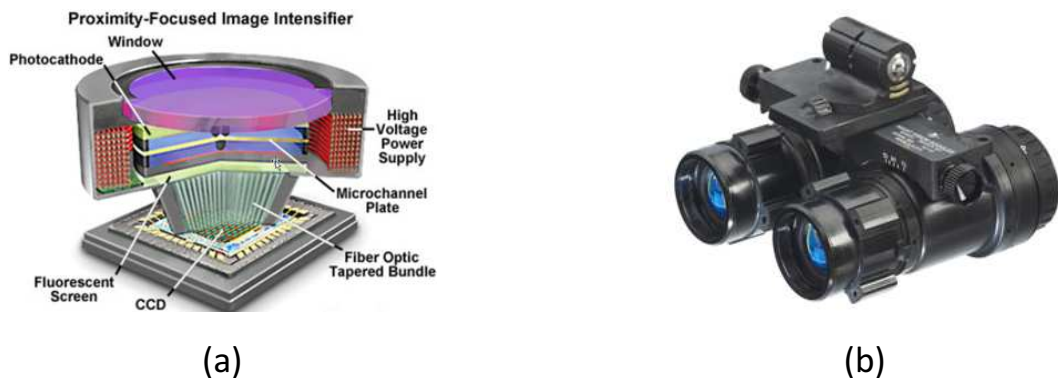


Fig. 15. Night vision device: (a) proximity-focused image intensifier and (b) Gen III night vision goggle AN/AVS-9 (ITT Night Vision).

Image intensifiers are widespread in many military applications. The advent of night-vision devices and helmet-mounted displays places additional constraints on the helmet, which is now an important element of the cockpit display system, providing weapon aiming, and other information—such as aircraft attitude and status—to the pilot. For example, figure 16 illustrates TopOwl® imaging system developed for airborne applications by Tales [16]. The Helmet Mounted Sight and Display incorporates a night vision system with a 100% overlapped projection of a binocular image on the visor. TopOwl® projects the night scene and associated symbology onto two circular reflective surfaces with a fully overlapped, 40-degree, binocular FOV. Standard symbology is used to display flight and weapon management data, helping to reduce crew workload.



Fig. 16. Tales TopOwl® helmet incorporate an optical combiner assembly for each eye, allowing the pilot to view the cockpit and the outside world directly with the night imagery superimposed on it. TopOwl® has a 40° FOV and a total headborne weight of 2.2 kg in full configuration. Reproduced from [16].

### *3.2 Thermal imaging systems*

The basic concept of a modern thermal imager system is to form a real image of the IR scene, detect the variation in the imaged radiation, and, by suitable electronic processing, create a visible representation of this variation analogous to conventional television cameras.

Due to existing terminology confusion in the literature, we can find at least 11 different terms used as synonyms of the earlier defined thermal imaging systems: thermal imager, thermal camera, thermal imaging camera, FLIR (forward looking infrared), IR imaging system, thermograph, thermovision, thermal viewer, infrared viewer, infrared imaging radiometer, thermal viewer, thermal data viewer and thermal video system. The only real difference between the above-mentioned terms is that the designations "thermograph", "infrared imaging radiometer" and "thermovision" usually refer to thermal cameras used for measurement applications, while the other terms refer to thermal cameras used in observation applications. For example, thermographic imagers supply quantitative temperature, while radiometers provide quantitative radiometric data on the scene (such as radiance or irradiance) or process these data to yield information about temperatures.

Thermal imagers have various applications, depending on the platform and user [17]. Most of them are used in military applications. They often have multiple fields of view that are user switchable during operation, which gives both a wide, general surveillance mode as well as a high magnification and narrow field for targeting, designating or detailed intelligence gathering. Many military thermal imagers are integrated with a TV camera and a laser range finder. A TV colour camera is used during daytime conditions due to its superior image quality. Nonmilitary uses include generic search and track, snow rescue, mountain rescue,

illegal border crossing detection and pilot assistance at night or in bad weather, forest fire detection, fire fighting, inspection and discreet surveillance as well as evidence gathering. A small but increasing group of thermal imagers enables noncontact temperature measurement and these cameras are used in areas of industry, science and medicine.

The term “focal plane array” (FPA) refers to an assemblage of individual detector picture elements (“pixels”) located at the focal plane of an imaging system. Although the definition could include one-dimensional (“linear”) arrays as well as two-dimensional (2D) arrays, it is frequently applied to the latter. Usually, the optics part of an optoelectronic images device is limited only to focusing of the image onto the detectors array. These so-called “staring arrays” are scanned electronically usually using circuits integrated with the arrays. The architecture of detector-readout assemblies has assumed a number of forms. The types of readout integrated circuits (ROICs) include the function of pixel deselecting, antiblooming on each pixel, subframe imaging, output preamplifiers, and may include yet other functions. Infrared imaging systems, which use 2D arrays, belong to so-called “second generation” systems.

The simplest scanning linear array used in thermal imaging systems consists of a row of detectors (figure 17(a)). An image is generated by scanning the scene across the strip using, as a rule, a mechanical scanner. At standard video frame rates, at each pixel (detector) a short integration time has been applied and the total charge is accommodated. A staring array is a 2D array of detector pixels (figure 17(b)) scanned electronically.

The scanning system, which does not include multiplexing functions in the focal plane, belongs to the first-generation systems. A typical example of this kind of detector is a linear photoconductive array (PbS, PbSe, HgCdTe) in which an electrical contact for each element of a multielement array is brought off the cryogenically cooled focal plane to the outside, where one electronic channel is used at ambient temperature for each detector element. The US common module HgCdTe arrays employ 60, 120 or 180 photoconductive elements depending on the application.

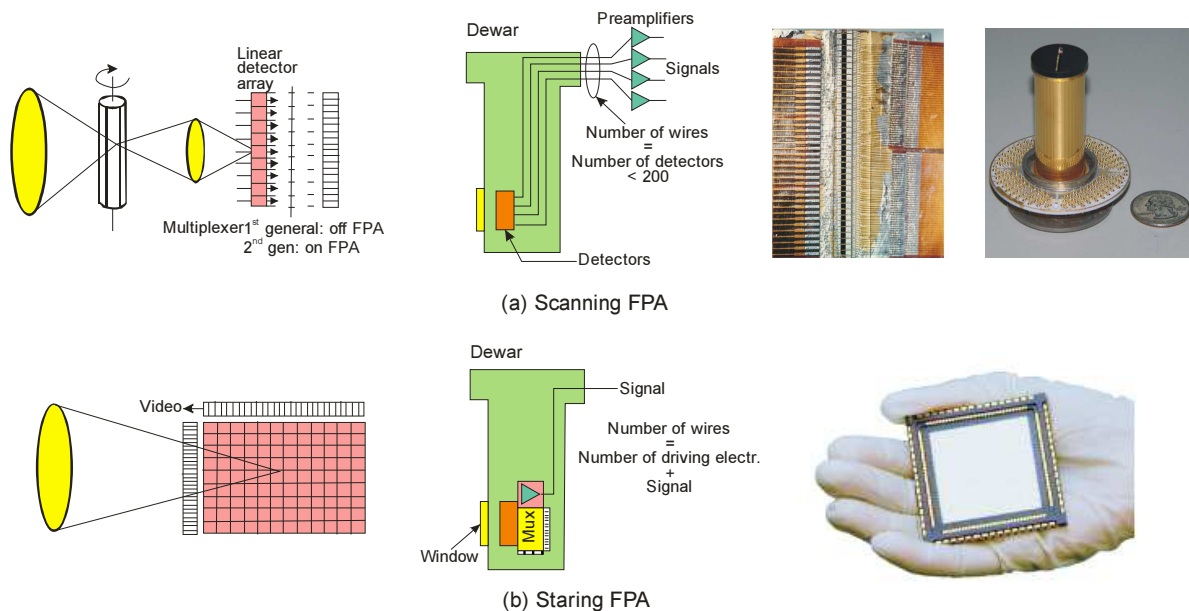


Fig. 17. Scanning and staring focal plane arrays.

The second-generation systems (full-framing systems), being developed at present, have at least three orders of magnitude more elements ( $< 10^6$ ) on the focal plane than first-generation systems and the detector elements are configured in a 2D array. These staring arrays are scanned electronically by circuits integrated with the arrays. These readout integrated circuits (ROICs) include, e.g. pixel deselecting, antiblooming on each pixel, subframe imaging,

output preamplifiers and some other functions. The optics merely focuses the IR image onto the matrix of sensitive elements.

Intermediary systems are also fabricated with multiplexed scanned photodetector linear arrays in use and as a rule, with time delay and integration (TDI) functions. Typical examples of these systems are HgCdTe multilinear 288×4 arrays fabricated by Sofradir, both for 3–5 and 8–10.5 μm bands with signal processing in the focal plane (photocurrent integration, skimming, partitioning, TDI function, output preamplification and some others).

A number of architectures are used in development of IR FPAs. In general, they may be classified as hybrid and monolithic ones, but these distinctions are often not as important as proponents and critics state them to be. The central design questions involve performance advantages versus ultimate producibility. Each application may favour a different approach depending on the technical requirements, projected costs and schedule.

In the monolithic approach (see figure 18(a)), some of the multiplexing is done in the detector material itself rather than in an external readout circuit. The basic element of a monolithic CCD devices is a metal–insulator–semiconductor (MIS) structure. An MIS capacitor detects and integrates the IR-generated photocurrent. Although efforts have been made to develop monolithic FPAs using narrow-gap semiconductors, silicon-based FPA technology with Schottky-barrier detectors is the only technology matured to a level of practical use.

Hybrid FPA detectors and multiplexers are fabricated on different substrates and are typically mated with each other by flip-chip bonding (figure 18(b)). In this case, we can optimize the detector material and multiplexer independently. Other advantages of the hybrid FPAs are near 100% fill factor and increased signal-processing area on the multiplexer chip. In the flip-chip bonding, the detector array is typically connected to the silicon multiplet pads by pressure contacts via indium bumps. The detector array can be illuminated from either the frontside or backside (with photons passing through the transparent detector array substrate). In general, the latter approach is most advantageous. When using opaque materials, substrates must be thinned to 10 μm in order to obtain sufficient quantum efficiencies and reduce the crosstalk. In some cases the substrates are completely removed.

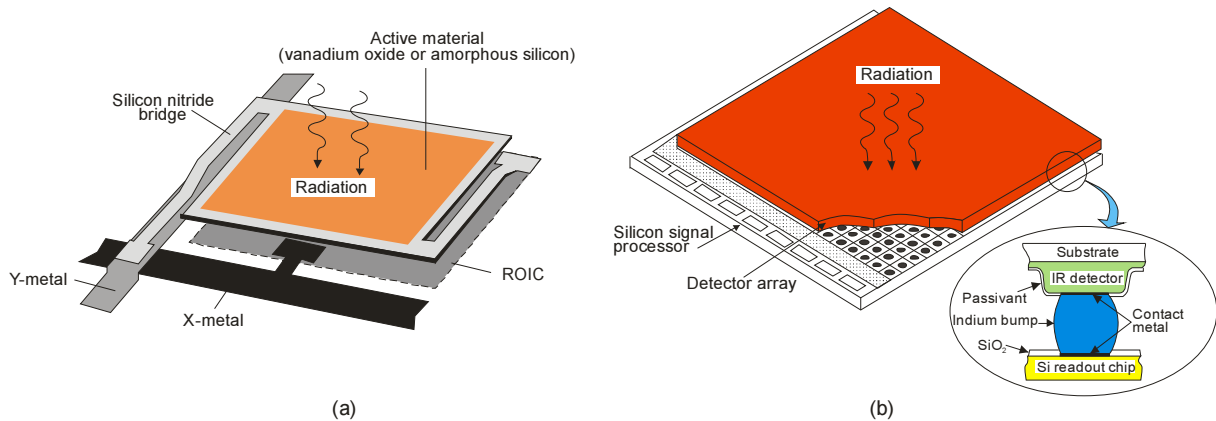


Fig. 18. Infrared focal plane arrays: (a) monolithic (microbolometer) and (b) hybrid.

Two types of silicon addressing circuits have been developed: CCDs and complementary metal–oxide–semiconductor (CMOS) switches. In CCD addressing circuits the photogenerated carriers are first integrated in the well formed by a photogate and subsequently transferred to slow (vertical) and fast (horizontal) CCD shift registers [19].

An attractive alternative to the CCD readout is coordinative addressing with CMOS switches. The configuration of CCD devices requires specialized processing, unlike CMOS imagers, which can be built on fabrication lines designed for commercial microprocessors.

CMOS have the advantage that existing foundries, intended for application specific integrated circuits (ASICs), can be readily used by adapting their design rules. Design rules of 14 nm are currently in production, with pre-production runs of 10 nm design rules. As a result of such fine design rules, more functionality has been designed into the unit cells of multiplexers with smaller unit cells, leading to large array sizes.

A typical CMOS multiplexer architecture consists of fast (column) and slow (row) shift registers at the edges of the active area, and pixels are addressed one by one through the selection of a slow register, while the fast register scans through a column, and so on. Each image-sensor is connected in parallel to a storage capacitor located in the unit cell. A column of diodes and storage capacitors is selected one at a time by a digital horizontal scan register and a row bus is selected by the vertical scan register. Therefore, each pixel can be individually addressed

The minimum resolvable difference temperature (*MRDT*) is often the preferred figure of merit for imaging sensors. This figure of merit comprises both resolution and sensitivity of the thermal imager. *MRDT* enables us to estimate probability of detection, recognition, and identification of targets knowing *MRDT* of the evaluated thermal imager. The *MRDT* is a subjective parameter that describes ability of the imager-human system for the detection of low contrast details of the tested object. It is measured as a minimum temperature difference between the bars of the standard 4-bar target and the background required to resolve the thermal image of the bars by an observer versus spatial frequency of the target (see figure 19). Military standards determining testing of the thermal imaging systems usually specify that *MRDT* values for a set of spatial frequencies of the tested imager must be lower than certain values if the imager is to pass the test. The measurement results of typical military thermal imagers for airborne surveillance are shown in figure 20.

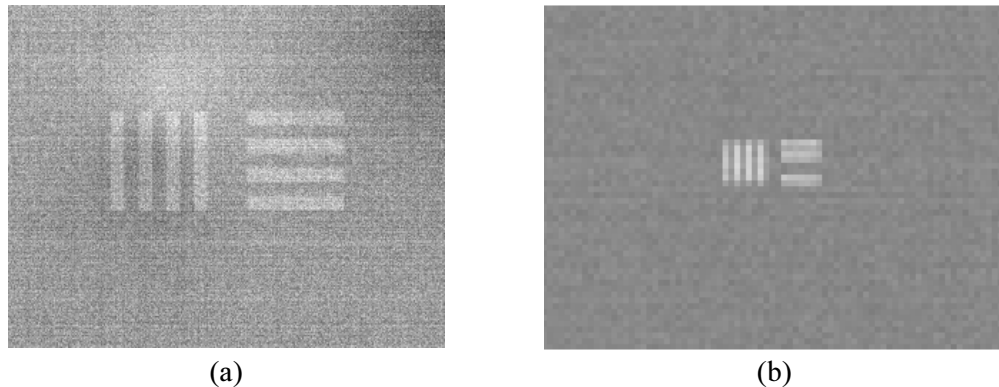


Fig. 19. Image of standard four-bar target during *MRDT* measurement: (a) target of low spatial frequency for low temperature difference and (b) target of high spatial frequency for high temperature difference between target and background (image magnified four times).

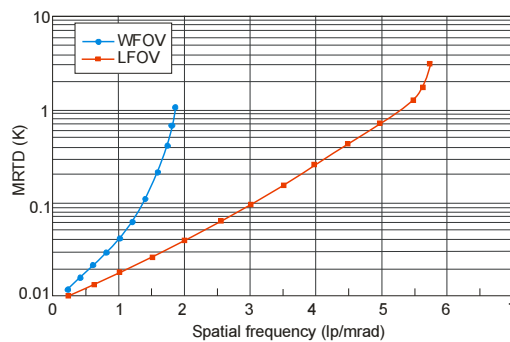


Fig. 20. *MRDT* of exemplary cooled staring thermal imager of two field of view (WFOV).

Nowadays classical *MRDT* is considered as the most important parameter of thermal imagers and is typically used for range predictions for real targets. However, it was reported



many times that the *MRTD* concept, when applied to undersampled imagers, generates incorrect range predictions; particularly the detection range. The biggest problem is low accuracy of performance modeling over Nyquist frequency.

There are at least three competing solutions to eliminate the above-mentioned limitation of *MRTD* concept and to improve accuracy of range prediction; namely, triangle orientation discrimination (*TOD*), minimum temperature difference perceived (*MTDP*), and dynamic *MRTD*. Therefore it can be expected that in future *MRTD* will be replaced by a new parameter as a main criterion for evaluation of thermal imagers.

### 3.3 IR cameras versus FLIR systems

Historically, a ‘camera’ includes neither the storage medium nor the display, while the ‘camera system’ includes the complete package. At present, manufacturers offer an optional recording medium (usually CD-ROM), display, and electronics for the display. For example, figure 21 is a photograph of the FLIR P660 IR. This camera has high resolution 640×480 thermal imagery with 30 mK sensitivity (*NEDT*), interchangeable lenses, and the flexibility of a tiltable, high-fidelity color LCD. The camera can be used by anyone who does numerous thermal inspections, or who needs to measure small objects from a great distance accurately.



Fig. 21. FLIR P660 IR camera.

Figure 22 shows representative camera architecture with three distinct hardware pieces: a camera head (which contains optics, including collecting, imaging, zoom, focusing, and spectral filtering assemblies), electronics/control processing box, and the display (see figure 9). Electronics and motors to control and drive moving parts must be included. The control electronics usually consist of communication circuits, bias generators, and clocks. Usually the camera sensor (FPA) needs cooling and therefore some form of cooler is included, along with its closed-loop cooling control electronics. Signal from the FPA is of low voltage and amperage and requires analog preprocessing (including amplification, control, and correction), which is located physically near the FPA and included in the camera head. Often, the A/D is also included here. For user convenience, the camera head often contains the minimum hardware needed to keep volume, weight, and power to a minimum.

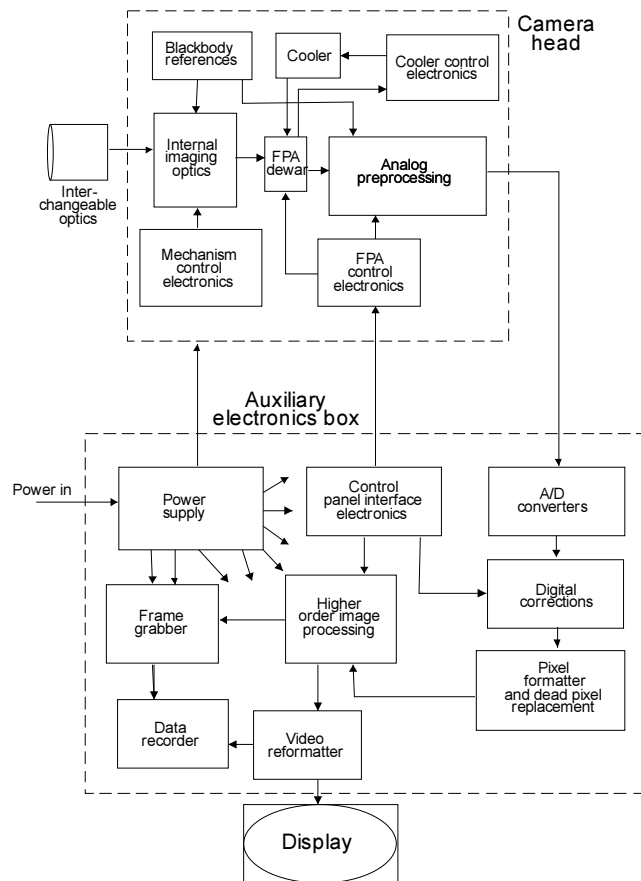


Fig. 22. Representative IR camera system architecture. Reproduced from [17].

Typical costs of cryogenically cooled imagers around \$50000 restrict their installation to critical military applications allowing conducting operations in complete darkness. A moving form cooled to uncooled operation (e.g. using silicon microbolometer) reduces the cost of an imager to below \$10000. Less expensive infrared cameras present a major departure from camera architecture presented in Fig. 22.

Cameras usually produce high-quality imagers with *NEDTs* of 20 – 50 mK. Details and resolution vary by optics and focal planes. A good camera produces an image akin to that of a black and white television.

‘FLIR’ is archaic 1960s jargon for forward-looking IR to distinguish these systems from IR line scanners, which look down rather than forward. Conversely, most sensors that do look forward are not considered to be FLIRs (e.g. cameras and astronomical instruments). The term ‘FLIR’ should be eliminated from IR techno-speak, but is still used and is likely to remain in the jargon for a while.

It is difficult to explain the difference between a camera and an FLIR system. In general, FLIRs are designed for specific applications and specific platforms, their optics is integrated into the package, and they are used mostly by people. Cameras usually rely on ‘imaging’ of a ‘target’ and they are designed for generic purposes, without much consideration for form and fit; they can be used with many different fore optics and are often used by computers and machines (not just people).

The term ‘FLIR’ usually implies military or paramilitary use, air-based units and scanners. The FLIR provides automatic search, acquisition, tracking, precision navigation and weapon delivery functions. A typical FLIR is comprised of four line replaceable units, such as an FLIR optical assembly mounted on a gyro-stabilized platform, an electronics module containing all necessary electronics circuits and a cryogenically cooled detector array, a power supply unit, and a control and processing assembly.

In the 1960s the earliest FLIRs were linear scanners. In the 1970s first-generation common modules (including a Dewar containing 60, 120 or 180 discrete elements of photoconductive HgCdTe) were introduced. The next generation of FLIRs employed a dense linear array of photovoltaic HgCdTe, usually  $2(4) \times 480$  or  $2(4) \times 960$  elements in TDI for each element. At present, these systems are replaced by full-framing FLIRs that employ staring arrays (HgCdTe, InSb and QWIP). For example, figure 23 shows eLRAS3 system (Long Range Scout Surveillance System) fabricated by Raytheon. eLRAS3 provides the real-time ability to detect, recognize, identify and geo-locate distant targets outside the threat acquisition. In addition, Raytheon's high-definition resolution FLIR (also called 3<sup>rd</sup> Gen FLIR) combines HgCdTe long-wave and mid-wave infrared arrays.



Fig. 23. 3rd Gen eLRAS3 FLIR system produced by Raytheon.

FLIRs are usually in several discrete packages referred to as line replaceable units (LRUs) such as: a scanner head, power supply, image processor, recorder, display and controls. They have the form of boxes spread around the host platform. The controls and display must be mounted in the cockpit with the humans. A representative FLIR architecture with the video signal output (to support LRU for image and higher-order processing) is shown in figure 24. Many systems depart significantly from the architecture of figure 24.

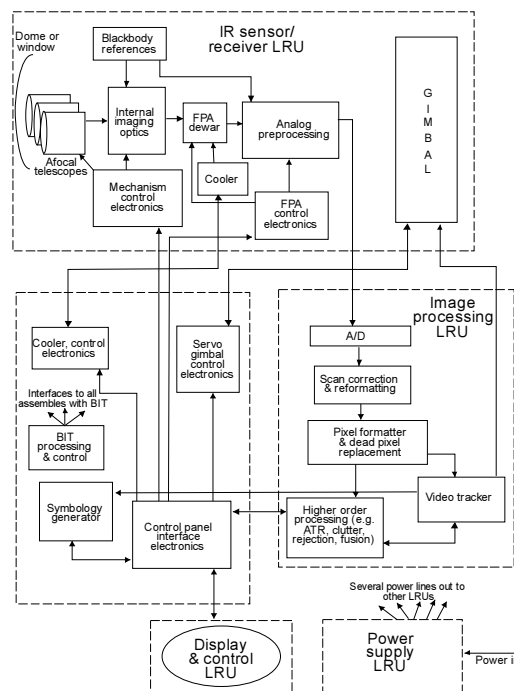


Fig. 24. Representative FLIR system architecture. Reproduced from [17].

FLIRs usually use telescopes in the sense that the lens system is focused at a distance considerably larger than the focal length. Characteristics such as field of view (FOV), resolution, element size and spatial frequency are expressed in angular units. By convention, FOV is expressed in degrees, resolution in milliradians, spatial frequency in cycles per milliradian and noise in units of temperatures.

Worldwide, there are several hundreds of different FLIR systems in operation. The most important of them are described in the literature [17,19]. Several FLIRs integrate a laser ranger or target designator.

Recent outgrowths of military FLIRs are the infrared search and track (IRST) systems. They are a subset or class of passive systems whose objective is to reliably detect, locate and continuously track IR-emitting objects and targets in the presence of background radiation and other disturbances. They are used in a radar-like manner (usually with a radar-like display) to detect and track objects. Most of the current research in IRST systems is concentrated in signal processing to extract target tracks from severe clutter.

Another group of outgrowths of military thermal imagers are airborne line scanners. These are one-dimensional scanning systems that enable creation of a two-dimensional thermal image of the observed scenery only when the system is moving. In contrast to typical thermal imagers with FOV not higher than about 40°, the airborne line scanners can provide FOV up to about 180°. Due to wide FOV airborne thermal scanners are widely used in military aerial reconnaissance.

### 3.4 Space-based systems

The formation of NASA in 1958, and development of the early planetary exploration programme, was primarily responsible for the development of the modern optical remote sensing systems, as we know them today. During the 1960s optical mechanical scanner systems became available that made possible acquisition of image data outside the limited spectral region of the visible and NIR available with film. 'Eye in The Sky' was the first successfully flown long-wavelength sensor launched in 1967. A major milestone was the development of the Landsat Multispectral Scanner because it provided the first multispectral synoptic in digital form. The period followed by the launch of Landsat-1 in 1972 stimulated the development of a new series of air- and spaceborne sensors. Since that time, hundreds of space-based sensors have been orbited.

The main advantages of space IR sensors are as follows [17]:

- the ability to tune the orbit to cover a ground swath in optimal spatial or temporal way;
- a lack of atmospheric effects on observation;
- global coverage;
- the ability to engage in legal clandestine operations.

Hitherto, anti-satellite weapons do not exist, so satellites are relatively safe from attack. The disadvantages of satellite systems are protracted and excessive costs of fabrication, launch and maintenance of satellites. Moreover, such operations as repair and upgrade are difficult, expensive and usually not possible.

The space-based systems installed on space platforms usually perform one of the following functions: military/intelligence gathering, astronomy, Earth environmental/resources sensing or weather monitoring. Thus, these functions can be classified as forms of Earth remote sensing and astronomy.

Figure 25 shows representative space sensor architecture. It should be stressed, however, that many individual space sensors do not have this exact architecture.

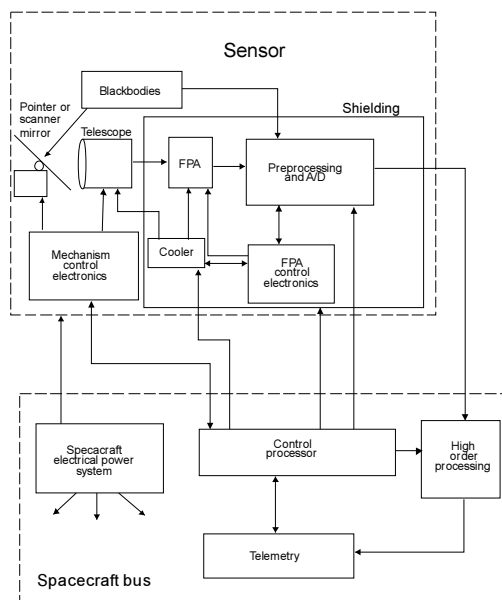


Fig. 25. Representative space sensor architecture. Reproduced from [17].

Intelligence and military services from wealthy nations have long employed space-based sensors to acquire information. A satellite-borne IR warning receiver, designed to detect intercontinental ballistic missiles, is a strategic system that protects a large area, or nation. The US spends about \$10 billion per year on space reconnaissance. Although the Cold War is over, the long-term strategic monitoring to assess the military and economic might is still important. Intelligence gathering of crop data and weather trends from the space has also been used by hunger relief organizations to forecast incidents of drought and famine more effectively. The military also has space-based surveillance for missile launches and additionally, space basing provides excellent viewing geometries for global events as nuclear explosions and environmental changes that the military is concerned about.

Imaging with IR FPAs provides increasingly detailed and quantitative information about relatively cool objects in the space of our galaxy and beyond. Dwarf stars, for example, or giant Jupiter-like planets in other distant solar systems, do not emit much visible and ultraviolet light, so they are extremely faint at these wavelengths. Also, longer IR wavelengths can penetrate dusty and optically opaque nebulous molecular clouds in interstellar space where new stars and planetary systems are forming.

There are several unique reasons for conducting astronomy in space [17]:

- to eliminate the influence of absorption, emission and scattering of IR radiation;
- to answer basic cosmological and astronomical questions (e.g. formation of stars, protoplanetary discs, extra-solar planets, brown dwarfs, dust and interstellar media, protogalaxies, the cosmic distance scale and ultra-luminous galaxies);
- to observe the Earth's environment (detecting the subtle changes indicating environmental stresses and trends).

NASA has historically been the leading US agency for promoting the development of long wavelength detector technologies. Figure 26 shows the sensitivities of currently-planned or active far-IR/sub-mm spectroscopic facilities in near future.

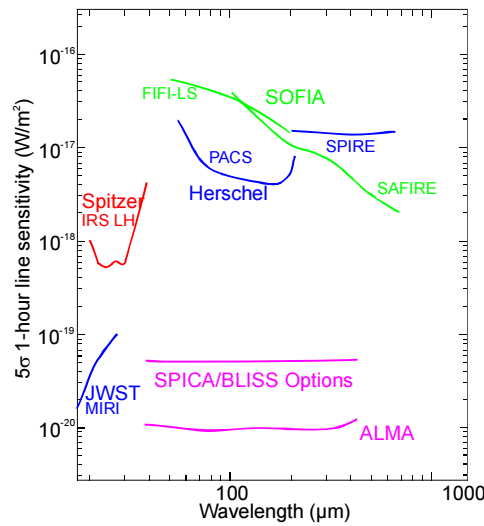


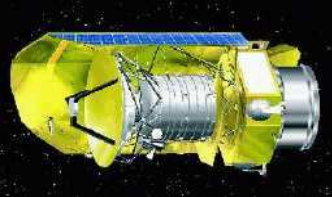


Fig. 26. Sensitivity of far-IR spectroscopy platforms. Reproduced from [20].

As the last figure shows, the James Webb Space Telescope (JWST) operates at wavelengths below about 27  $\mu\text{m}$ . The Atacama Large Millimeter/submillimeter Array (ALMA) operating through a number of submillimeter atmospheric windows as well as  $\sim 650 \mu\text{m}$ , will have sensitivities at least 100 times higher than Herschel spanning the intervening 60–650  $\mu\text{m}$  wavelength range. ALMA and JWST are currently scheduled to start operations within the next few years. The Space Infrared Telescope for Cosmology and Astrophysics (SPICA), with launch envisioned in 2017, will provide two-to-three orders of magnitude increase in sensitivity in comparison with Herschel that will bring far-IR/sub-mm sensitivity into line with those of JWST and ALMA. The ambitious requirements of future space missions are summarized in table 6.

Table 6. Far-IR spectroscopy platforms.

<p><b>Spitzer</b> <b>Space</b> <b>Telescope</b>  <b>2003</b></p>		<p>The <b>Spitzer Space Telescope</b> was launched in August 2003. It is the last of NASA's "great observatories" in space. Spitzer is much more sensitive than prior infrared missions and studies the universe at a wide range of infrared wavelengths. Spitzer concentrates on the study of brown dwarfs, super planets, protoplanetary and planetary debris disks, ultraluminous galaxies, active galaxies, and deep surveys of the early universe.</p>
<p><b>SOFIA</b>  <b>2005</b></p>		<p><b>SOFIA (Stratospheric Observatory For Infrared Astronomy)</b> was finally completed in 2005. SOFIA, a joint project of NASA and the German Space Agency, incorporates a 2.5-meter optical/infrared/sub-millimeter telescope mounted in a Boeing 747. Designed as a replacement for the successful Kuiper Airborne Observatory, SOFIA is the largest airborne telescope in the world.</p>
<p><b>Herschel Space</b> <b>Observatory</b>  <b>2009</b></p>		<p>The <b>Herschel Space Observatory</b> carried into orbit in May 2009, is a European Space Agency infrared-submillimeter mission. Herschel is performing spectroscopy and photometry over a wide range of infrared wavelengths and is used to study galaxy formation, interstellar matter, star formation and the atmospheres of comets and planets. The Herschel Observatory is capable of seeing the coldest and dustiest objects in space. It is the largest space telescope ever launched carrying a single mirror of 3.5 meters in diameter.</p>

ALMA

2011



The **Atacama Large Millimeter/submillimeter Array (ALMA)** is an international partnership between Europe, North America, East Asia and the Republic of Chile to build the largest astronomical project ever. It is an astronomical interferometer, comprising an array of 66 12-meter and 7-meter diameter radiotelescopes observing at millimeter and submillimeter wavelengths. It is being built on the Chajnantor plateau at 5000 meters altitude in the Atacama desert of northern Chile. ALMA is expected to provide insight on star birth during the early universe and detailed imaging of local star and planet formation. Costing more than a billion dollars, it is the most ambitious ground-based telescope currently under construction. ALMA began scientific observations in the second half of 2011 and was scheduled to be fully operational by the end of 2012.

James Webb  
Space  
Telescope

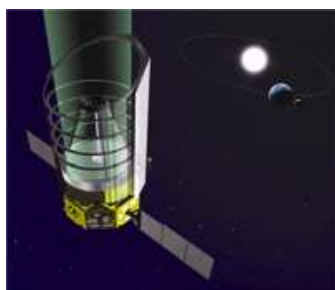
2018



The **James Webb Space Telescope (JWST)** is a large, infrared-optimized space telescope, scheduled for launch in 2018. It is a visible/infrared space mission which will have extremely good sensitivity and resolution, giving us the best views of the sky ever in the near-mid infrared. JWST will be used to study the early universe and the formation of galaxies, stars and planets. Webb will have a large mirror, 6.5 meters in diameter and a sunshield the size of a tennis court. Both the mirror and sunshade will not fit onto the rocket fully open, so both will fold up and open once Webb is in outer space. Webb will reside in an orbit about 1.5 million km from the Earth.

SPICA/BLISS

2017



The **Background-Limited Infrared-Submillimeter Spectrograph (BLISS)** is a far-IR spectrograph concept for **Space Infrared Telescope for Cosmology and Astrophysics (SPICA)**. The SPICA mission is a future Japanese infrared astronomical satellite, with the launch envisioned in 2017, to explore the universe with a cooled, large telescope.

The philosophy of BLISS is to provide a rapid survey spectroscopy capability over the full far-IR range. The baseline approach is a suite of broadband grating spectrometer modules with transition-edge superconducting (TES) bolometers. SPICA will use a cooled telescope (3.5 m diameter primary, ~5 K) to achieve sensitivities currently inaccessible to existing facilities operating over this wavelength range (SOFIA, Herschel).

### 3.5 Smart weapon seekers

A seeker is a primary homing instrument for smart weapons that include missiles, bombs, artillery projectiles, and standoff cruise missiles. They are developed to increase accuracy of munitions.

Taking into account the use of electromagnetic spectrum, smart weapon seekers can be divided into:

- electro-optical seekers,
- microwave seekers, and
- radio controlled seekers.

Below, electro-optical seekers that dominate in group of short range smart munitions are discussed.

Electro-optical seekers are basically homing instruments that use optical radiation in the range from far-infrared to ultraviolet. The most popular group of electro-optical seekers employ infrared radiation. However, seekers that use visible or UV band can be met, too. More advanced seekers can use several spectral bands of electromagnetic radiation: infrared/UV, infrared/microwave, etc.

In general, seekers can be divided into two groups:

- passive seekers, and
- active seekers.

Passive seekers do homing using optical radiation emitted by the target or using radiation emitted by natural sources and reflected by the target. Next, passive seekers can be further divided into two basic groups: non-imaging seekers and imaging seekers. Active seekers use

optical radiation emitted by external platforms or by themselves to irradiate the target and carry out homing.

Passive non-imaging seekers use circular optical plate with adjacent transparent and non-transparent parts, called a reticle, that is fixed at the image plane of the imaging optics of the head of a missile (figure 27). A single IR detector of the size a little larger than the reticle is placed just behind it. Location of the point image of the target on the reticle plate changes, even when the target does not change its position, due to rotation of the reticle or rotation of the imaging optics. Therefore radiation emitted by the target generates electrical pulses at the detector output. Pulse duration and phase of these pulses give information about the angular position of the target (figure 28).

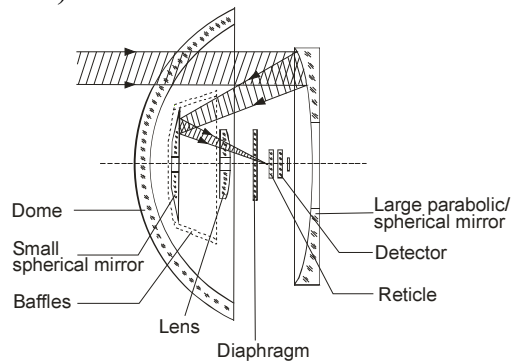


Fig. 27. Optical diagram of a typical passive non-imaging seeker.

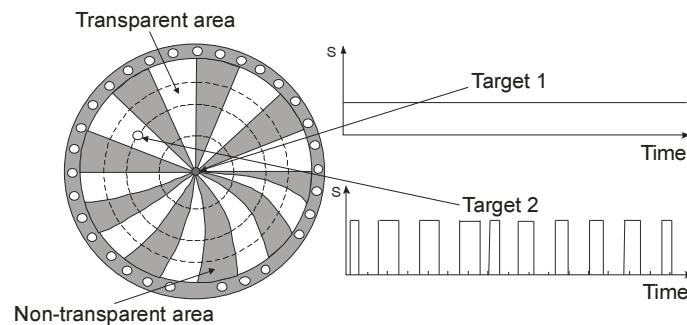


Fig. 28. Exemplary reticle and the signal generated at the detector output by a few targets of different location.

The grandfather of passive IR seekers - the Sidewinder seeker developed in the 1950s – was a passive non-imaging seeker; it employed vacuum tubes and a lead salt single-element detector. During the next decades it was found that, despite their simplicity, passive non-imaging seekers were very effective for guiding missiles when the target was on a uniform background. Therefore, at present, the majority of currently used short-range smart missiles use this type of seekers. However, the effectiveness of passive non-imaging seekers decreases significantly for targets on non-uniform background like typical ground military targets or in presence of countermeasures. Thus, the trend of future systems is toward passive imaging seekers.

Passive imaging seekers typically have a thermal imager (SWIR camera or VIS/NIR camera) in their optoelectronic head. Location of a target is determined from analysis of the image generated by the imaging module. Thermal imagers or SWIR imagers are preferred solutions due to their ability to generate high contrast images in difficult atmospheric conditions. VIS/NIR cameras are rarely used due to vulnerability to atmospheric conditions and problems to recognize low contrast targets. The most advanced imaging seekers use in fact two imaging modules: MWIR imager and SWIR imager or MWIR imager and UV imager.

A representative architecture of a staring seeker is shown in figure 29. To keep low the seeker volume, weight and power requirements, only the minimum hardware needed to sense the scene is included. We can note that the seeker's output is going to a missile-based



processor, behind the FPA in the seeker, to perform tracking and aim point selection. The concept of the seeker's operation includes a standby turn-on, followed by a commit, which cools the FPA. At the beginning, the seeker is locked onto its target by an external sensor or a human. Next, the missile is launched and flies out locked onto its target, matching any target movement. Finally, when the target is close and imaged, the missile chooses an aimpoint and conducts final manoeuvres to get to the target or selects a point and time to fuse and explode.

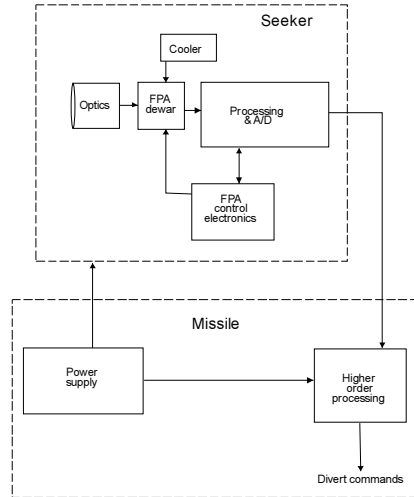


Fig. 29. Representative imaging (staring) seeker architecture. Reproduced from [17].

Due to the use of advanced image analysis, imaging seekers can attack targets located in non-uniform background in presence of advanced countermeasures. Thus, some of modern air-to-ground missiles use this method to attack and destroy ground targets; particularly large non-movable targets like bridges, bunkers, buildings, etc. However, there are some technological challenges. First, it is difficult to design small size, reliable MWIR/SWIR imagers capable of generating high quality images under harsh environmental conditions met in most smart munitions (ultra high acceleration, extreme temperatures). Second, there is also a commercial challenge in the design of passive imaging seekers as such seekers, being disposable devices, cannot be too expensive. Therefore, imaging modules used in passive imaging seekers are often strongly simplified versions of typical thermal imagers/SWIR imagers or UV imagers used for surveillance applications. Imaging modules that generate low resolution image (below  $320 \times 240$  pixels – see figure 30) are frequently met. Due to above mentioned technological problems, the passive imaging based MWIR/SWIR/UV modules in their optical heads are still rarely found and continue to be at a development stage.



Fig. 30. Image of aircraft generated by low resolution MWIR imager ( $128 \times 128$  pixels).

Active electro-optical seekers typically use lasers that operate in SWIR range (1064 nm or in 1550 nm band). These lasers emit radiation that irradiate the target of interest and enable homing on this target.

Active laser guided seekers can be divided into two subclasses according to the method of homing. The first group are seekers homing on the target irradiated by a target designator using radiation reflected by the target (figure 31(a)). The second group constitute seekers homing on a target indicated by a target designator using radiation of laser beam that irradiates back of the seeker head (figure 31(b)).

Seekers homing on the target irradiated by pulsed laser designators are the most popular group of active electro-optical seekers. These seekers enable very accurate location of small targets in a highly non-uniform background and are particularly well suited for air-to-ground missiles or bombs. However, warning systems or other countermeasures can significantly reduce the effectiveness of such seekers because it is relatively easy to detect an object illuminated by pulsed laser radiation.

Seekers irradiated with a laser beam are kept on their flight to the target within the beam emitted by the laser designator that irradiates the target. Laser radiation, which gives information on target location, comes directly from the illuminator to the sensors at the back of the missile, not after the reflection by the target as in the previous method. Therefore, low-power designators can be used here and the effectiveness of the warning systems is reduced. However, a big drawback of this group of seekers is the fact that the seeker must be guided by aircraft that shoot the missile until it hits the target.

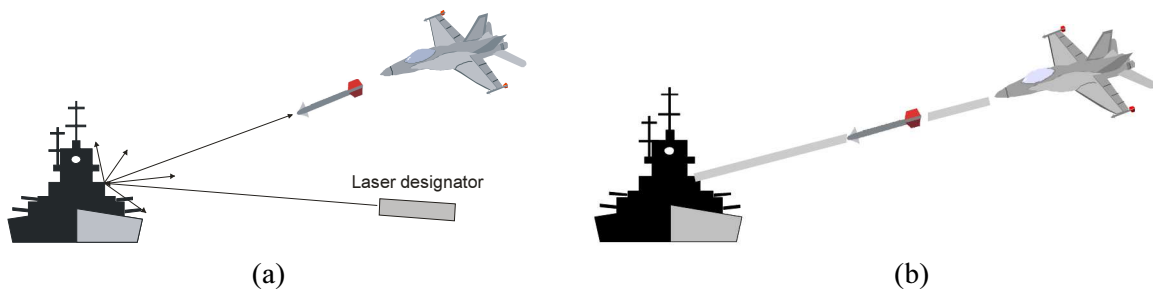


Fig. 31. Principle of work of active laser guided seekers: (a) seeker homing on the irradiated target and (b) seeker irradiated with a laser beam).

Munitions, and particularly missiles, that use smart seekers, are very expensive. A typical price is over the level of one hundred thousand US \$, sometimes even amounting to millions of US \$. It is a fair price for using such disposable weapons to destroy enemy aircraft, helicopters and tanks but there are doubts about economic sense of using such expensive weapons in asymmetric wars against lightly armoured guerillas. Therefore, low cost smart munitions make a noticeable trend in smart weapon technology. Another big trend is seekers of improved intelligence capable of finding a true target against modern countermeasures. Dual passive imaging seekers that employ two spectral bands (MWIR/LWIR or MWIR/UV) to eliminate countermeasures are first of examples of new more advanced seekers. Active laser seekers that combine classical laser homing methods with an additional imaging module are another example of a new generation of advanced smart seekers.

The new generation of standoff weapons relies on real-time target recognition, discrimination, tracking, navigation and night vision. It is predicted that smart weapons will tend to replace the radar emphasis as stealth platforms are increasingly used for low-intensity conflicts. It is more difficult to perform IR missile warning than radar guided missile warning.

#### 4. Noncontact thermometers

Infrared thermometers always measure temperature indirectly in two stages [21]:

- measurements of radiation power in one or more spectral bands;
- determination of an object temperature on the basis of the measured radiometric signals.

Even simple IR thermometers usually consist of five or more blocks (see figure 32). An optical objective is usually used to increase the amount of radiation emitted by the tested object and to limit thermometer FOV. The signal at the output of the detector is typically amplified, converted into a more convenient electronic form and finally digitized. A separate visualization block is typically used for presentation of the measurement results.

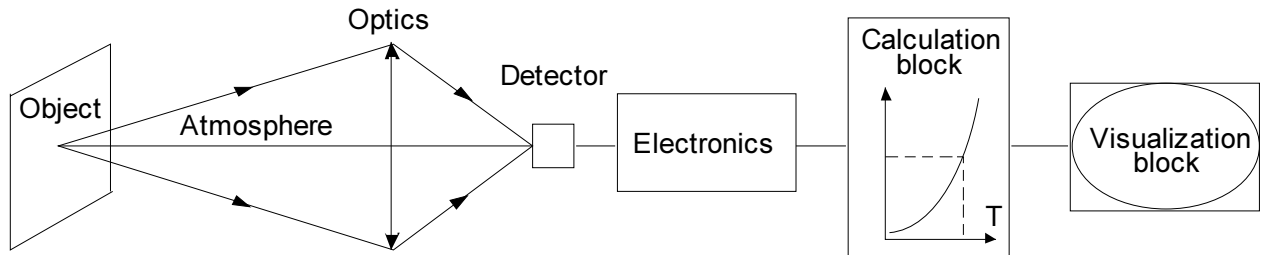


Fig. 32. General diagram of a simple noncontact thermometer.

The IR thermometers can be divided into a few groups according to different criteria: presence of an additional co-operating source, number of system spectral bands, number of measurement points, width of system spectral bands and transmission media.

In a passive system, the object temperature is measured taking into account the radiation power emitted by the object in one or more spectral bands. With an active system we can get some information about the emissive properties of the tested object by using an additional co-operating source that emits radiation directed to the tested object and measuring the reflected radiation. They are active systems. Active thermometers are more sophisticated, more expensive and so far only in a few applications can they really offer better accuracy than passive systems. Therefore, nowadays, almost all practical noncontact thermometers are passive ones.

In the passive single-band systems, the object temperature is determined using a system calibration chart derived from radiometric calculation of the output signal as a function of blackbody temperature. The temperature of nonblackbody objects can be corrected only if their emissivity over the spectral band is known.

The ratio of the power emitted by a greybody at two different wavelengths does not depend on the object emissivity but only on the object temperature. In passive dual-band systems, the object temperature is usually determined using a calibration chart that represents the ratio of the emitted power in two bands as a function of the object temperature.

At present, at least 99.9% of systems available commercially on the market are passive single-band systems; passive dual-band systems are rather rarely used; passive multiband systems are still at a laboratory stage of development.

According to the number and location of measurement points, the infrared thermometers can be divided into pyrometers, line scanners and thermal cameras.

Pyrometers enable temperature measurement of only a single point or rather of a single sector (usually a circle or a square) of the surface of a tested object (see figure 33(a)). Line scanners enable temperature measurement of many points located along a line. Scanners are typically used to measure temperature of moving objects (see figure 33(b)). Due to the movement of the target of interest the scanners can create a two-dimensional image of temperature distribution on the surface of a tested object. Thermal cameras enable temperature measurement of thousands of points located typically within a rectangle or square and create a 2D image of temperature distribution on this area.

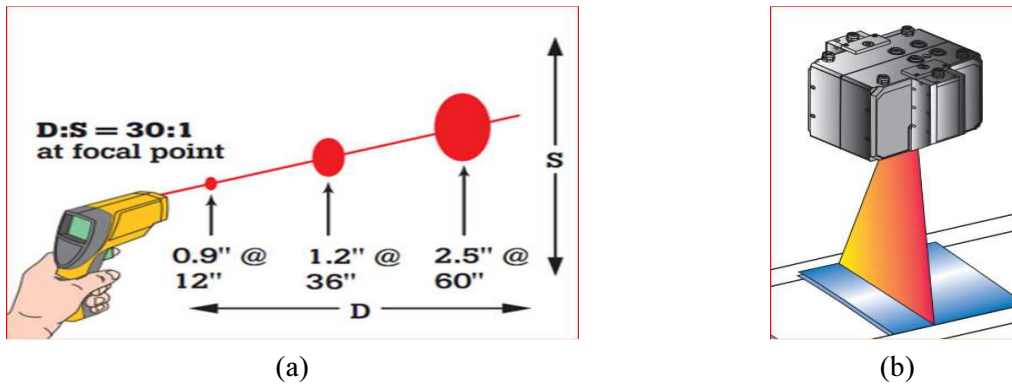


Fig. 33. Principle operation of: (a) pyrometer and (b) line scanners.

Most commercially available noncontact thermometers are pyrometers. They are small, light and low-cost systems that have found numerous applications in industry, science, etc. Majority of them are hand-held, quasi universal devices integrated with a laser sight as shown in figure 34(a) [22]. On the market, there are also compact, rugged, industrial pyrometers optimized for harsh industrial conditions (see figure 34(b)).



Fig. 34. Photos of two pyrometers: (a) Fluke 62 handheld pyrometer (<http://www.fluke.com>) and (b) Land IQ industrial pyrometer.

Pyrometers offer noncontact temperature measurement in the range from about  $-40^{\circ}\text{C}$  to over  $2000^{\circ}\text{C}$  using different spectral bands from LWIR band to ultra narrow bands in visible or near infrared ranges. The most numerous pyrometers are devices optimized for measurement of low temperatures (from about  $-20^{\circ}\text{C}$  to about  $250^{\circ}\text{C}$ ) using thermopile detectors.

Line scanners are especially suitable for temperature measurement of moving objects and have found applications in the automotive industry, welding, robotics, etc. Unlike pyrometers - that measure a single point - line scanners measure very quickly multiple temperature points across a scan line, with high resolution and in ultra wide FOV. On the market can be found line scanners able to offer measurement of 150 line per second, with 1024 pixels in a single line, and in  $90^{\circ}$  FOV (see Fig. 35) [23]. High measurement speed, high image resolution and ultra wide FOV are the reasons why line scanners are able to withstand a competition with thermal cameras.

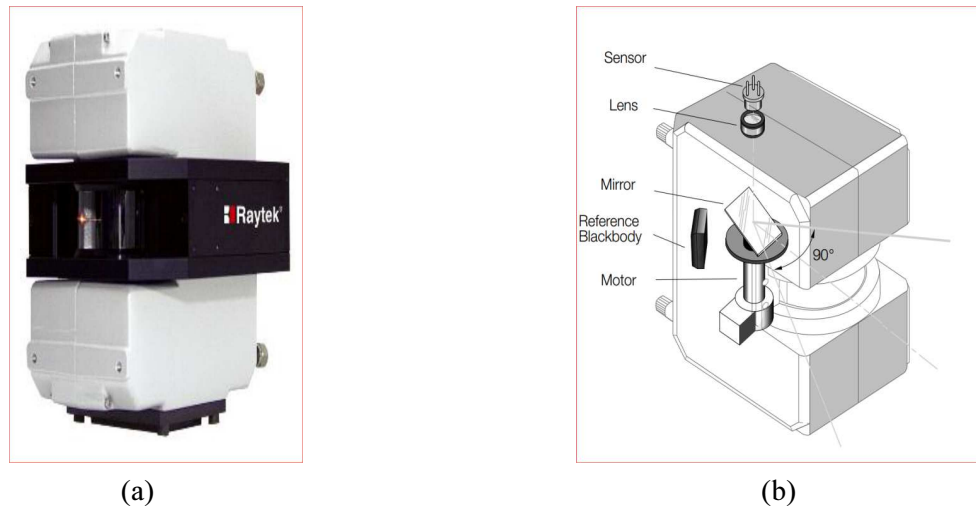


Fig. 35. MP150 line scanner from Raytek: (a) photo block and (b) diagram.

Thermal cameras offer the greatest number of capabilities of all discussed types of noncontact thermometers. For several decades high price was a factor that significantly limited mass applications of thermal cameras. In the past thermal cameras were divided onto two basic groups: MWIR thermal cameras based on thermoelectrically/Stirling/liquid nitrogen cooled FPAs sensitive in 3–5- $\mu\text{m}$  spectral band and LWIR thermal cameras based on Stirling/liquid nitrogen cooled FPAs sensitive in 8–12- $\mu\text{m}$  band. MWIR cameras were more frequently found due to the lower cost of sensors.

At the beginning of the 2000s, the appearance of low cost LWIR noncooled arrays (microbolometers) has completely changed the situation. Nowadays, market is totally dominated by noncooled LWIR thermal cameras (see figure 36) [24, 25]. These cameras have found numerous applications such as control of electrical supply lines, heat supply lines, civil engineering, environmental protection, nondestructive testing and many others. Cooled thermal cameras built using MWIR or LWIR FPAs are mostly met in high end expensive applications like spectral selective measurement of metals, polymers, glasses, through flames, etc.



Fig. 36. Photos of two thermal cameras: (a) VigoCAM5 thermal camera built using 640×480 LWIR array of bolometers and (b) MSC640 thermal camera built using NIR CMOS imaging sensor.

LWIR/MWIR thermal cameras can potentially enable measurement of temperature up to 3000°C but cameras that operate at SWIR/NIR spectral range can offer much lower internal measurement errors at higher temperatures over about 400°C. The cost of SWIR cameras is much higher than the cost of VIS/NIR cameras built using low cost CMOS/CCD sensors. Therefore, thermal cameras using a narrow spectral band in NIR range dominate among thermal cameras optimized for testing targets at high temperatures over about 600°C (see figure 36(b)). The latter thermal cameras should be treated as special versions of typical CCD/CMOS cameras optimized for radiometric measurements.

It should be noted that LWIR/MWIR thermal cameras dedicated for noncontact temperature measurements differ significantly from LWIR/MWIR thermal cameras for surveillance applications. Different FPA sensors, different electronics and optics are typically used for design of thermal cameras that belong to these two groups. Moreover, the speed of measurement thermal cameras is typically kept below about 9 frame per seconds to fulfil requirements on thermal cameras for non military applications kept by export control agencies.

Noncontact thermometers understood as pyrometers, line scanners and thermal cameras represent a technology that has found mass application in almost every form of human activities. Number of these devices sold on the market is increasing every year. Price vary from several dozens of US \$ for some simple pyrometers, to tens of thousands of US \$ for high end thermal cameras.

The last warning is that in spite of a high number of available thermometers, accurate non contact measurement of temperature is a real challenge in many applications. The reason is that internal errors of typical noncontact temperature meters are relatively low, i.e. below 1–2%. However, external errors due to improperly estimated emissivity of a tested object, radiation reflected by this object, or due to non corrected atmospheric attenuation and emission, can be ten times (or more) higher than the internal errors. Therefore, at least basic knowledge about methods of noncontact temperature measurement is crucial to keep these external errors at a minimal level.

## **5. Radiometers**

In general, the infrared thermometers discussed in section 4 can be treated as a class of radiometers because they determine temperature on the basis of the signal generated by the radiant flux coming to the detector. However, the infrared thermometers are designed to measure only temperature and it is usually not possible to use them to measure radiant flux. In our definition, a radiometer is an instrument designed to measure quantities of optical radiation or radiant properties of materials in optical range from UV to far IR. It should be noted that photometric meters can be considered as specific radiometers optimized to measure quantities of visible radiation (light) when receiving sensor simulates spectral sensitivity of a human eye. However, photometers are excluded from the further analysis.

The optical radiometers can be divided into several groups according to three main criteria:

- number of measured quantities,
- number of spectral bands,
- number of measurement points.

A universal radiometer should enable measurement of a long list of quantities of optical radiation (radiant power, radiant energy, radiant intensity, radiance, irradiance, radiant exposure) and measurement of radiant properties of materials (like emissivity, reflectance and transmittance) in a set of spectral bands of optical radiation (UV, VIS, NIR, SWIR, MWIR, LWIR, VLWIR).

It is technically possible to develop a universal radiometric system. However, such a test system would be bulky, modular, composed from many blocks, and extremely expensive. Therefore, there are no truly universal radiometers on the market. Nevertheless, semi-universal radiometric systems of more limited performance are commonly met on the market. These radiometers are based on a concept of a quasi-universal electronic meter with several exchangeable optical heads (see figure 37).

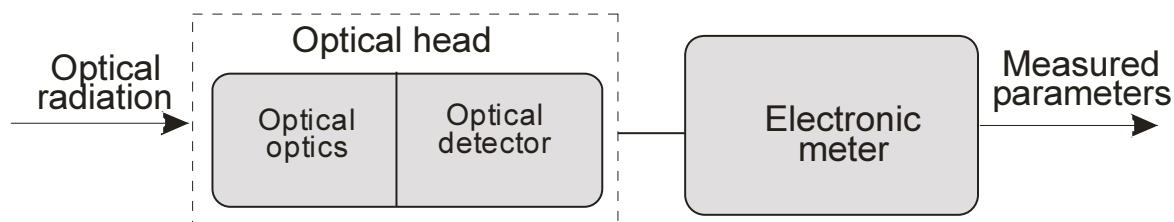


Fig. 37. Block diagram of a typical semi-universal optical radiometer.

Optical meters capable of measuring power, pulse energy, irradiance of VIS/NIR/SWIR radiation are the prime example of radiometers from the latter group (see figure 38). Their extreme versatility is achieved by a modular approach coupled with an extensive selection of accessories and powerful application software packages, which enables the user to tailor a turn-key system to their exact requirements as well as insure expandability in the future. Another even more popular type of radiometers are specialized, compact optical meters optimized to measure a single optical quantity (power meters, pulse energy meter, wavelength meters, etc.).



Fig. 38. PM320E optical meter produced by Thorlabs Inc: (a) photo of universal electronic meter and (b) photo of several optical heads.

According to the criterion of the number of spectral bands, the optical radiometers can be divided into four groups: single-band radiometers, dual-band radiometers, multiband radiometers, and spectroradiometers.

Optical meters equipped with an optical head based on a single detector can be considered as single-band radiometers. If an optical meter is equipped with several optical heads of different spectral bands, then such a device can be considered as a dual or multi-band radiometer. When the spectral bands are narrow and their number is high enough, then the multiband radiometers are termed spectroradiometers. In contrast to a situation in non-contact thermometry, where multi-band thermometers are very rarely met, the spectroradiometers are a popular group of optical radiometers and have found a wide area of applications.

The key component of any spectroradiometer is a module that can be termed a spectral band selector. Its task is to select the desired spectral band from the incoming radiation. This task is achieved by means of several methods: variable wavelength filters, monochromators, and Fourier Transform (FT) interferometers.

The transmission wavelength of circular (linear) variable filters changes continuously (discretely) with the position of the fraction of the filter. Simplicity of design is a great advantage of this type of spectroradiometers – it enables design of small size, reliable, high speed and mobile systems. However, using the variable filters it is not possible to achieve good spectral resolution; resolution of spectroradiometers built using variable filters is not better than about 2% of the wavelength.

A monochromator is an optical instrument that uses a dispersing component (a grating or a prism) and transmits to the exit slit (optionally directly to the detector) only a selected spectral fraction of the radiation incoming to the entrance slit. The centre wavelength of the transmitted spectral band can be changed within the instrument spectral region by rotation of the dispersing element. Very good spectral resolution can be achieved using grating monochromators (as high as 0.1% of wavelength). However, the monochromator transmits the optical radiation only in a very narrow spectral band. Moreover, grating monochromators are designed using low speed optics. As a result, the optical detectors at the output of monochromators receive only a very small fraction of radiation incoming to the monochromator input. Therefore, spectroradiometers built using grating monochromators suffer poor sensitivity. Cooled optical detectors of ultra high sensitivity are often used in such a type of spectroradiometers to reduce the earlier mentioned drawback, however with a limited effect.

The Michelson interferometer is the spectral band selector in FT spectroradiometers. The interferometer is usually built as an optical instrument consisting of a beam splitter and two flat mirrors arranged so as to recombine the two separated beams back on the same spot at the beam splitter. One of the mirrors moves linearly in order to produce variable optical interference (see figure 39(b)) [26].



Fig. 39. The ABB MB3000 Series FT-IR Laboratory Analyzer: (a) photo and (b) schematic block diagram (<http://www.abb.com>).

The Michelson interferometer can also be seen as a modulator. From a constant spectral radiation input, a temporal modulation occurs at the detector having a unique modulation frequency for each wavelength of radiation. The modulation frequency can be scaled via the velocity of the mirror movement. This modulated signal registered by the detector is called an interferogram. It is digitised at the rate of at least twice the maximum modulation frequency and a mathematical operation, the Fourier transform, is applied to retrieve the spectral distribution of the input radiation. A calibration with a known source is required in order to obtain quantitative radiometric results.

FT spectroradiometers are characterized by very good spectral resolution and very good sensitivity, better than offered by spectroradiometers built using grating monochromators or variable wavelength filters. These features enable design of high-speed, high spectral resolution FT spectroradiometers using non-cooled or thermoelectrically cooled detectors (typically HgCdTe detectors) instead of bulky liquid nitrogen cooled detectors needed in the variable filter or dispersive spectroradiometers. Therefore, FT spectroradiometers have found mass applications in many areas, but are particularly numerous as spectral analysers in industry.

Performance of the FT spectroradiometers can be severely reduced even by a very small non-alignment of the optical system, which makes them inherently sensitive to shocks and vibrations. That is why, in the last few decades, FT spectroradiometers have been considered



rather as a laboratory type of equipment that cannot be used in field applications. However, at present this opinion is outdated as on the market there are fully mobile FT spectroradiometers that can be used in military, meteorological, and environmental applications.

From the point of view of measuring points, all radiometers can be divided onto two basic groups: spot radiometers and imaging radiometers.

Great majority of the commercially available radiometers are systems enabling measurement of the spectral distribution of radiation emitted/reflected or transmitted by a single spot and these systems can be termed as spot radiometers. The radiometers that have been discussed so far belong to this group. The second group are imaging radiometers that generate images at one or more spectral bands and can be further divided into: single-band, dual band, multi-band, multispectral, and hyperspectral imaging radiometers.

Basically all electro-optical imagers (thermal imagers, SWIR imagers, VIS/NIR cameras, UV cameras) designed to measure absolute distribution of radiance on the surface of an analysed target can be considered as single-band imaging radiometers.

Surveillance satellites are often equipped with multi-band imaging radiometers that offer two-dimensional images of the Earth at several spectral bands, e.g. visible, near infrared, and long wavelength infrared. These imaging radiometers are often built as several single band imaging radiometers that share common broadband optics.

Multispectral imaging radiometers are a special subgroup of multiband imaging devices, which offer images at significant number of relatively narrow spectral bands, but the spectral bands do not form a continuous spectrum. Landsat satellites are good examples of multispectral multiband imaging radiometers. Landsat 8 satellite can deliver images in eleven spectral bands from visible to far infrared (see table 7) [27]. It must be noted that there are some empty spectral regions that are not covered by Landsat 8 satellite.

Table 7. Spectral bands of Landsat 8 satellite.

No	Name of spectral band	Wavelength (micrometers)
1	Coastal aerosol	0.43 – 0.45
2	Blue	0.45 – 0.51
3	Green	0.53 – 0.59
4	Red	0.64 – 0.67
5	Near Infrared	0.85 – 0.88
6	SWIR 1	1.57 – 1.65
7	SWIR 2	2.11 – 2.29
8	Panchromatic	0.50 – 0.68
9	Cirrus	1.36 – 1.38
10	Thermal infrared (TIRS) 1	10.60 – 11.19
11	Thermal infrared (TIRS) 2	11.50 – 12.51

Hyperspectral imaging radiometers are the most advanced subgroup of multiband imaging radiometers, which deliver two-dimensional images at such a high number of narrow spectral bands that they form a continuous spectrum. In other words, these imaging radiometers deliver a spectrum for each pixel of generated images. The output data is typically shown in the form of so-called hyperspectral cubes ( $x, y, \lambda$ ), where  $x, y$  are spatial coordinates and  $\lambda$  is wavelength (see figure 40) [28].

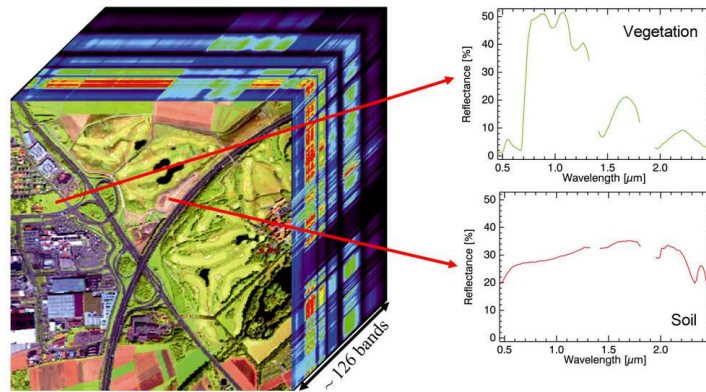


Fig. 40. Hyperspectral data cube acquired with imaging hyperspectral radiometer HyMap®.

Hyperspectral imaging radiometers can be designed using four distinct methods of acquiring hyperspectral cubes  $(x, y, \lambda)$ :

- spatio-spectral scanning,
- spatial scanning,
- spectral scanning, and
- non-scanning.

Spectral scanning system and spatial scanning system are needed in hyperspectral imaging radiometers built using the spatio-spectral scanning method. An imaging radiometer built as a scanning grating monochromator with a linear imaging detector at its exit slit moving in space can be treated as an example of this method. The radiometer originally generates only a linear spatial image at a single wavelength but a two-dimensional spatial image is achieved by movement of the radiometer; and data about the complete spectrum is achieved due to scanning of the grating monochromator. Very long time period is needed to acquire a two-dimensional spatial image at the complete spectrum (complete hyperspectral cube  $(x, y, \lambda)$  for all combinations of the coordinates  $x, y, \lambda$  like shown in figure 40) because spectral scanning along  $\lambda$  axis must be repeated for many discrete spatial values of  $y$  axis assuming that linear detector is oriented along  $x$  axis. The acquisition time can be shortened many times if both spectral scanning and spatial scanning work at the same time, but then this method generates an incomplete hyperspectral cube  $(x, y, \lambda)$  because information about all combinations of  $x, y, \lambda$  is not delivered.

Hyperspectral imaging radiometers built using spatial scanning method need only a spatial scanning system that creates a two-dimensional spatial image from an original one-dimensional spatial image. A non-scanning grating monochromator with a 2D imaging detector at its exit plane moving in space is an example of this method. This imaging detector captures a spectrally dispersed image of a linear target. A two-dimensional image of a scenery of interest is achieved by movement of the radiometer. This method is particularly suited for space radiometers due to their natural movement relative to the Earth.

Hyperspectral imaging radiometers built by using spectrally tuneable optical filter placed before FPA are an example of radiometers using spectral scanning. At one discrete moment of time this imaging radiometer generates a complete 2D image of the observed scenery. Spectral scanning due to filter tuning generates a series of such 2D spatial images for different wavelengths.

Different types of optical tuneable filters are used: liquid crystal, acousto-optic, or thin-film filters tuneable by adjusting the angle of incidence. Light weight, small dimensions and low power requirements are a big advantage of imaging radiometers built using tuneable optical filters. However, these imaging radiometers suffer from rather poor sensitivity, poor spectral resolution, and too narrow spectral band. These disadvantages are not present in imaging FT spectroradiometers that can be also considered as a special case of imaging

radiometers built using the spectral scanning method. These imaging spectroradiometers generate a 2D spatial image of a scene of interest and an interferogram for each pixel of this image. Mathematical transformations of the acquired image data generate a hyperspectral 3D cube as shown in figure 41 [26].

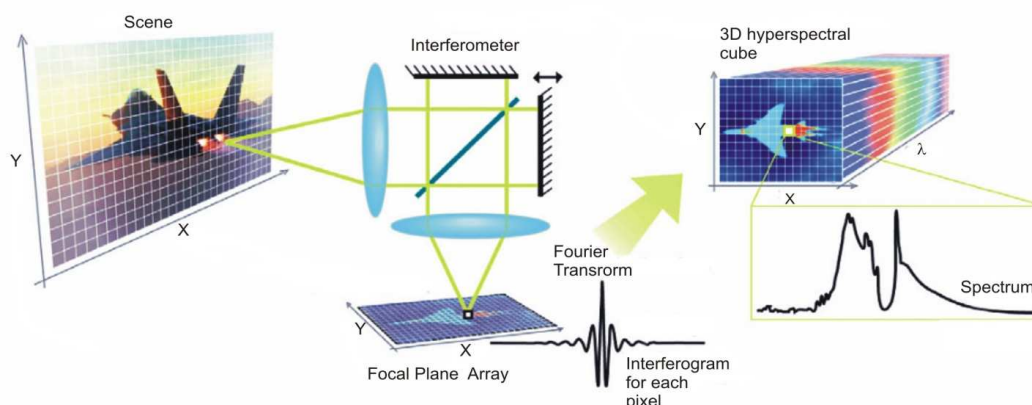


Fig. 41. Spectral scanning method used by hyperspectral imaging FT spectroradiometers.

Spectral scanning in FT imaging spectroradiometers is indirectly done by movement of a mirror in an interferometer. A captured interferogram can be converted using Fourier transform into spectrum. FPA receives full spectrum emitted by a scene of interest and such feature makes this method particularly sensitive. Ultra high spectral resolution and wide spectral ranges can be achieved, too.

The spectral scanning method is optimal for typical applications at Earth conditions where both the radiometer and the target are static or are moving but not along a desired axis. Therefore, these imaging radiometers dominate on the market.

All three methods discussed so far need a relatively long time (hundreds times more than time needed to create a single image frame by electronic imaging sensors) to generate the hyperspectral cube and this long acquisition time is a significant disadvantage of these methods. The non-scanning method can potentially deliver complete a 3D hyperspectral cube at a time period comparable to the integration time of electronic imaging sensors (below 50 ms). Next, non-scanning hyperspectral imaging radiometers can potentially measure spectrum of the scenery that emits low amount of optical radiation due to higher light efficiency. This method called "snapshot hyperspectral imaging" can potentially bring a revolution in hyperspectral imaging comparable to replacement of scanning thermal imagers based on discrete/linear IR detectors to staring thermal imagers built using two dimensional IR FPAs [29]. However, there are many technological problems to implement this method practically in commercial products. So far, there is a significant interest in non-scanning imaging radiometers but there are no such imaging radiometers offered on the international market.

As it was stated earlier, successful design of non-scanning hyperspectral imaging radiometers is a big technological challenge. However, design of scanning hyperspectral imaging radiometers is difficult, too. Hyperspectral imaging radiometers differ significantly from non-imaging spectroradiometers. The former systems must use a modified optical system with the corrected curved output field and astigmatism to generate sharp images of the input slit corresponding to the wavelength focused on different parts of the array detector, which enables simultaneous measurement of the spectrum. There are also big differences in the complexity of electronics and software needed for data processing. Thus, hyperspectral imaging can be considered as the most technologically challenging part of optical radiometry.

## 6. Light detection and ranging (LIDAR)

LIDAR is an acronym for light detection and ranging, an active optical remote technique in which a beam of light is used to make range-resolved measurements. The LIDAR emits a light beam that interacts with the medium or object under study in much the same way that a sonar uses sound pulses, or a radar uses radio waves. In a radar, radio waves are transmitted into the atmosphere, which scatters some of the power back to the radar's receiver. Similar to radar technology, the range to an object is determined by measuring the time delay between transmission of a pulse and detection of the reflected signal. The LIDAR also transmits and receives electromagnetic radiation, but at a higher frequency. The analysis of the backscattered light allows some property of the medium or object to be determined. LIDARs operate in the ultraviolet, visible and IR region of the electromagnetic spectrum. Typically, wavelengths vary to suit the target from about 10 micrometers to approximately 250 nm.

LIDAR is popularly used as a technology to make high-resolution maps, with applications in agriculture, geomatics, archeology, geography, geology, seismology, forestry, physics and astronomy (remote sensing and metrology), etc. Few military applications are known to be in place and are classified, but a considerable amount of research is underway in their use for imaging. Higher resolution systems collect enough detail to identify targets, such as tanks. Examples of military applications of LIDAR include the airborne laser mine detection system for counter-mine warfare. At present LIDAR systems are also used to do stand-off detection for the discrimination of biological warfare agents and to provide the earliest possible standoff warning of a biological attack.

LIDAR was developed in the early 1960s, shortly after the invention of the laser, and it was initially used for mapping particles in the atmosphere. During the 1980s, the development of GPS opened up the applications to moving sensors (airborne LIDAR). The early 1990s saw the ability to begin achieving decimetre accuracies.

In the LIDAR approach, a laser radiation is transmitted into the atmosphere and backscattered radiation is detected as a function of time by a optical receiver. The return time of the reflected or scattered pulses provides range information. In a LIDAR arrangement, the backscattered light is collected by a telescope, usually placed coaxially with the laser emitter. The signal is then focused on a photodetector through a spectral filter, adapted to the laser wavelength.

A LIDAR instrument can be conveniently divided into three subsystems [30]: the transmitter, the receiver, and the detector (see figure 42). The transmitter is the subsystem that generates light pulses and directs them into the atmosphere. The receiver collects and processes the scattered laser light and then directs it to a photodetector. The signal detection and recording section takes the light from the receiver system and produces a permanent record of the backscattering intensity, and possibly wavelength and/or polarization, as a function of altitude. In modern LIDARs, detection and recording are achieved electronically.

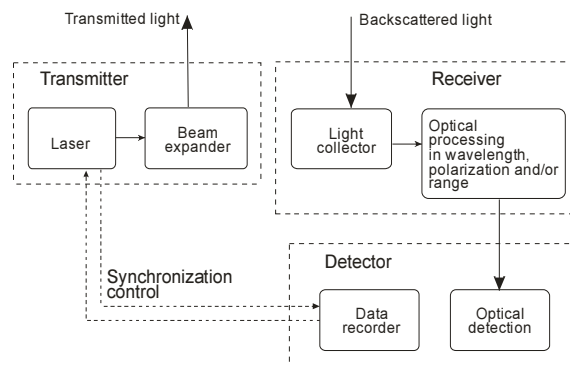


Fig. 42. Schematic of a simple LIDAR.

Different kinds of laser are used depending on the power and wavelength required. The lasers may be both cw or pulsed. Inexpensive lasers emitting light in the spectral range between 0.6 and 1.0 microns are most common for non-scientific LIDAR applications. Their maximum power is limited by the need to make them eye-safe (visible light can be focused and is easily absorbed by the eye). Eye-safety is often a requirement for most applications. A common alternative are 1.55- $\mu\text{m}$  lasers, which are eye-safe at much higher power levels since this wavelength is not focused by the eye. Airborne topographic mapping LIDARs generally use 1.064- $\mu\text{m}$  diode pumped YAG lasers, while bathymetric systems generally use 0.532- $\mu\text{m}$  frequency doubled diode pumped YAG lasers (this light penetrates water with much less attenuation than does 1.064  $\mu\text{m}$ ). Laser settings include the laser repetition rate, which controls the data collection speed. Better target resolution is achieved with shorter pulses, provided the LIDAR receiver detectors and electronics have sufficient bandwidth.

In general there are two kinds of LIDAR detection schemes: "incoherent" or direct energy detection (which is principally an amplitude measurement) and coherent detection (which is best for Doppler, or phase sensitive measurements). Coherent systems being more sensitive than direct detection, allow them to operate a much lower power but at the expense of more complex transceiver requirements.

Two main photodetector technologies are used in LIDARs: solid state photodetectors, such as silicon avalanche photodiodes or photomultiplier (visible and UV). 3D imaging can be achieved using both scanning and non-scanning systems. "3D gated viewing laser radar" is a non-scanning laser ranging system that applies a pulsed laser and a fast gated camera. Imaging LIDAR can also be performed using arrays of high speed detectors and modulation sensitive detector arrays typically built on single chips using CMOS and hybrid CMOS/CCD fabrication techniques. Using this technique many thousands of pixels/channels may be acquired simultaneously.

Airborne topographic LIDAR systems are the most common LIDAR systems used for generating digital elevation models for large areas. The combination of an airborne platform and a scanning LIDAR sensor is an effective and efficient technique for collecting elevation data across tens to thousands of square miles. A basic LIDAR system involves a laser range finder reflected by a rotating mirror. The laser is scanned around the scene being digitised, in one or two dimensions, gathering distance measurements at specified angle intervals. The schematic idea shown in figure 43 is fairly straightforward [31]: measure the time that it takes a laser pulse to strike an object and return to the sensor (which itself has a known location due to direct georeferencing systems), determine the distance using the travel time, record the laser angle, and then, from this information, compute where the reflecting object (e.g., ground, tree, car, etc.) is located in three dimensions.

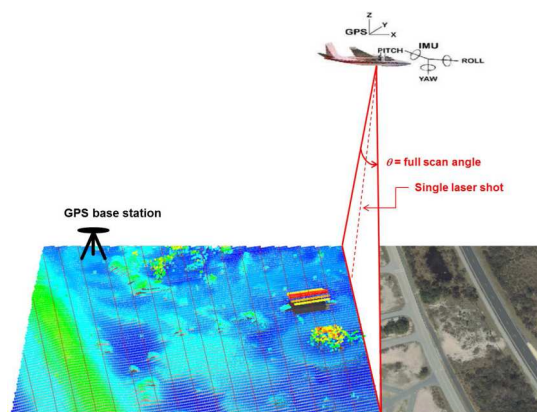


Fig. 43. Schematic diagram of airborne lidar performing line scanning resulting in parallel lines of measured points.

LIDAR systems allow scientists and mapping professionals to examine both natural and manmade environments with accuracy, precision, and flexibility. For example, figure 44 shows LIDAR collected by the National Oceanic and Atmospheric Administration (NOAA) survey aircraft (top) over Bixby Bridge in Big Sur, California [32]. Here, LIDAR data reveals a top-down (bottom left) and profile view of Bixby Bridge.

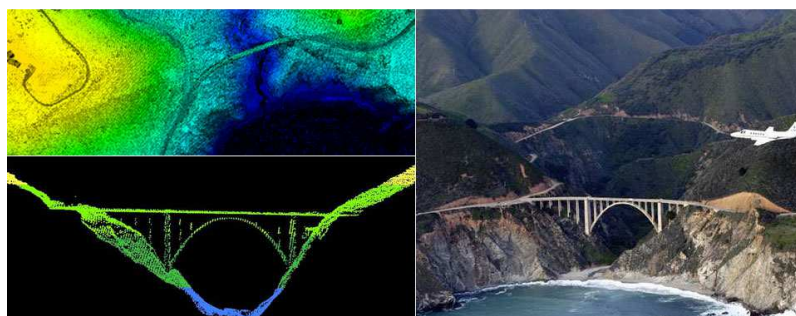


Fig. 44. LIDAR data is often collected by NOAA survey aircraft (top) over Bixby Bridge in Big Sur, California.

Typically light is reflected via backscattering. Different types of physical process in the atmosphere are related to different types of light scattering. Choosing different types of scattering process allows atmospheric composition, temperature and wind to be measured. The scattering is essentially caused by Rayleigh scattering on nitrogen and oxygen molecules, Mie scattering on aerosols (dusts, water droplets, etc), Raman scattering, and fluorescence. At low altitudes, Mie scattering is predominant because of the higher cross-section and the high aerosol concentration. Based on different kinds of backscattering, the lidar can be accordingly called Rayleigh LIDAR, Mie LIDAR, Raman LIDAR, Na/Fe/K Fluorescence LIDAR, and so on. Suitable combinations of wavelengths can allow for remote mapping of atmospheric contents by identifying wavelength-dependent changes in the intensity of the returned signal.

In general, a signal is produced by either direct absorption, fluorescence or Raman scattering. Absorption techniques are most straightforward and widely applied. In the atmosphere, for example, long-path absorption spectrometry is used in two wavelength bands — the infrared, where many molecules have characteristic fingerprints, and the ultraviolet (UV) to the visible range.

In a typical case, the laser is alternatively tuned to a wavelength within the absorption band of interest (at  $\lambda_{on}$ ) and then to a wavelength with negligible absorption (at  $\lambda_{off}$ ), so that the difference in the signal returned either from a surface or from air- or water-borne particles is recorded. By dividing the two LIDAR signals by each other, most troublesome and unknown parameters are eliminated and the gas concentration as a function of the range along the beam can be evaluated. Such applications require tuneable lasers, either tuneable diode lasers in the IR or Nd:YAG dye lasers in the UV to visible range.

Differential absorption LIDAR (DIAL) measurements utilize two or more closely spaced ( $< 1$  nm) wavelengths to factor out surface reflectivity as well as other transmission losses, since these factors are relatively insensitive to wavelength. When tuned to the appropriate absorption lines of a particular gas, DIAL measurements can be used to determine the concentration (mixing ratio) of that particular gas in the atmosphere.

The principle for differential absorption LIDAR (DIAL) is schematically represented in figure 45. May it be assumed that wavelength couple ( $\lambda_{on}$ ,  $\lambda_{off}$ ) is sent simultaneously into the atmosphere. As  $\lambda_{on}$  and  $\lambda_{off}$  have been chosen close enough to exhibit the same scattering properties, the first chimney plume will cause an increase in the backscattering signal, because the concentration of aerosols is larger, but the same increase for both pulses. Conversely, the second chimney plume, which contains a certain quantity of the pollutant, will absorb the backscattered signal at the  $\lambda_{on}$ -wavelength much more strongly than at the  $\lambda_{off}$

-one. From this difference, and using the Beer-Lambert law, one can deduce the specific concentration of the pollutant under investigation versus the range. For typical pollutants, such as sulfur dioxide, nitrous oxide, ozone and mercury, detection ranges for the part-per-billion detection level are between 0.5 and 5 km.

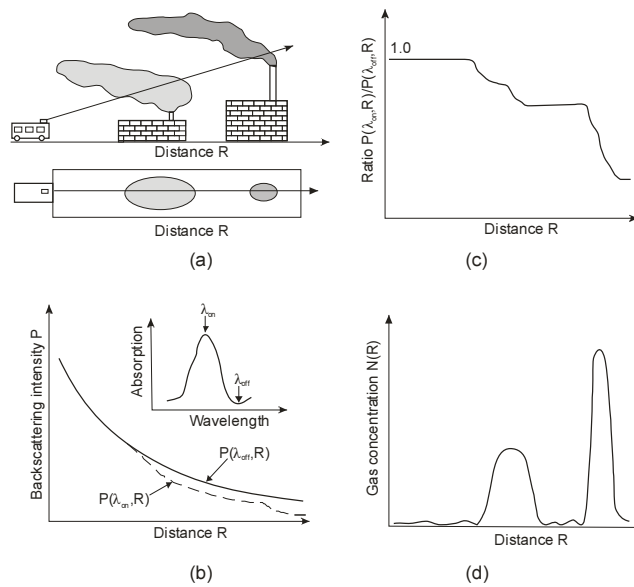


Fig. 45. Illustration of the principle of different absorption LIDAR (DIAL): (a) pollution measurement situation, (b) back-scattered laser intensity for the on- and off-resonance wavelengths, (c) ratio (DIAL) curve and (d) evaluated gas concentration. Reproduced from [33].

The main alternative to direct-absorption spectrometry is Raman scattering. This occurs when photons are inelastically scattered from molecules, exciting them in the process and releasing some photon energy. Thus, Raman return signals are at a different, longer wavelength than the exciting wavelength. Raman cross-sections are much smaller than absorption cross-sections, so the Raman technique works well using high-power lasers only for higher concentrations (hundreds of parts per million) and distances of less than 1 km. Water vapour profiles can be obtained in vertical soundings up to several kilometres in height, and pressure profiles up to tens of kilometres are measurable using Raman signals from atmospheric  $N_2$ .

The other major technique, fluorescence spectrometry, has a limited use in atmospheric measurement because the return signal is too weak. The technique is, however, an excellent way to monitor solid targets in the biosphere, such as oil, spills, algae bloom patches and forest areas. The fluorescent signal from plants originates in the excitation of chlorophyll and other leaf pigments. Fluorescence LIDAR is also a powerful technique for measurements at mesospheric heights where the pressure is low and the fluorescence is not quenched by collisions. This technique has been used extensively to monitor layers of various alkali and alkaline earth atoms (Li, Na, K, Ca and  $Ca^+$ ) at a height of about 100 km [33, 34].

In addition to monitoring pollutants, LIDAR is widely used to measure wind velocities via Doppler shifts. The improved laser stability has expanded LIDAR to more ambitious projects, including the study of winds in the stratosphere. Also, Doppler systems are now beginning to be successfully applied in the renewable energy sector to acquire wind speed, turbulence, wind veer and wind shear data.

The main advantage of LIDAR is that it can map the location of chemicals over a wide region. Due to the rapid nature of laser pulses, the time resolution is critical (a few nanoseconds) to get good spatial resolution. Overall, DIAL systems can provide 2D or 3D information of air pollutants. However, most of the existing LIDAR systems have not met the

pragmatic deployment requirements of users in industry or government. LIDAR systems are usually complex, large, expensive and require highly skilled personnel for their operation.

## 7. IR gas sensors

The late 19<sup>th</sup> and early 20<sup>th</sup> century saw the observation spectra of various gases, even the resolving of the rotational fine structure associated with certain simple molecules. Measurements were, however, very difficult due to the lack of suitable devices. A major advance occurred with the development of non-dispersive IR (NDIR) technique in 1943 [35], when useful IR detectors became available (in the 1950s), and after the development of a multilayer thin film interface filter for wavelength selection in the infrared (in the 1950s). At present, IR gas detection is a well-developed measurement technology. In general, these instruments are among the most user-friendly ones and require the least amount of maintenance.

Optical gas detection using absorption spectroscopy is based on the application of the Beer-Lambert law;

$$I = I_0 \exp(-\alpha l), \quad (11)$$

where  $I$  is the light transmitted through the gas cell,  $I_0$  is the light incident on the gas cell,  $\alpha$  is the absorption coefficient of the sample (typically with units of  $\text{cm}^{-1}$ ) and  $l$  is the cell's optical pathlength (typically with units of cm). The absorption coefficient  $\alpha$  is the product of the gas concentration (for example in atm – the partial pressure in atmospheres) and the specific absorptivity of the gas (for example in  $\text{cm}^{-1}\text{atm}^{-1}$ ). Typical absorption spectra for five gases in IR spectral region are shown in figure 46.

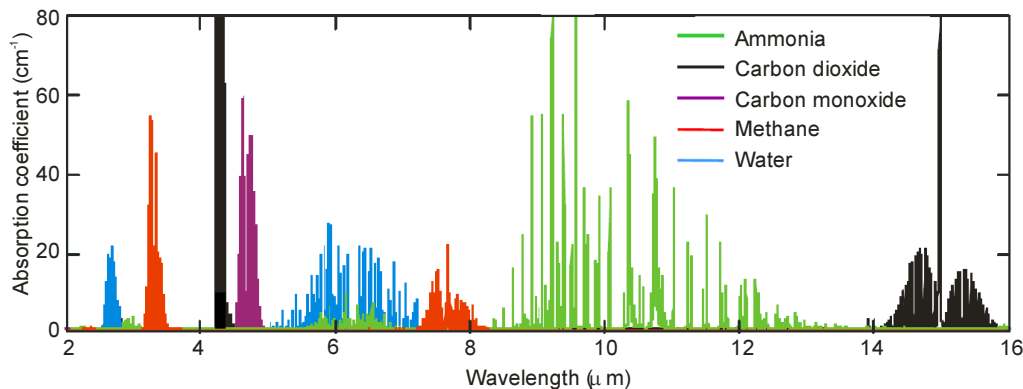


Fig. 46. Absorption spectra for five gases in the mid IR region of the spectrum (all at 100% vol).

The Beer-Lambert law applies for monochromatic radiation; when using light sources that are broader than absorption lines, the width of the source must be accounted for. The law also assumes that there are no chemical changes in the sample - at high concentrations, dimer formation can alter spectra, but this is a minor effect for most gases at a standard temperature and pressure.

The most commonly used techniques in gas sensing based on measurement of optical absorption at specific wavelengths are: NDIR technique, spectrophotometry, tuneable diode laser spectroscopy (TDLS) and photoacoustic spectroscopy (PAS) [36].

A non-dispersive infrared sensor, commonly referred to simply as an infrared sensor, is not susceptible to poisons, can detect gases in inert atmospheres, and be made very specific to a particular target gas. The limitation of NDIR technology for gas detection is dependent on the uniqueness of the absorption spectrum of a particular gas. NDIR sensors are also extremely stable, quick to respond to a gas and can tolerate long calibration intervals. Infrared sensors



are commonly used to detect methane, carbon dioxide and nitric oxides in both portable and fixed gas detection instrumentation.

There are a number of ways by which various IR components can be arranged to produce a gas analyser. Infrared gas sensors utilise only a part of the IR spectrum, corresponding to wavelengths which are absorbed by the gas to be detected. The optical bandwidth of a laser source is sufficiently narrow for it to be used directly, but with wideband sources, as thermal sources or even LEDs, some additional wavelength selection in the optical path is required. The optical bandwidth of a sensor is typically in the tens or hundreds of nanometres to match to the absorption band of the gas. Wavelength selection is achieved using dispersive elements such as prisms or diffraction gratings, or a non-dispersive element such as a multilayer thin film filter.

The design may be relatively simple, or very complicated depending on the type of an analyser for the applications. Figure 47 illustrates some of the basic features of IR analysers.

The basic design is shown in figure 47(a), which consists of an IR source, bandpass filter and the interaction with the gas sample and detector. A detector is selectively sensitized to the absorption wavelength of the gas whose presence is to be detected by the use of a narrow-bandpass optical filter. Clearly then, increased gas concentration in the optical path between the source and the filtered detector leads to a depression in the signal level. The bandpass filter could be placed in front of the light source, instead of placing it in front of the detector.

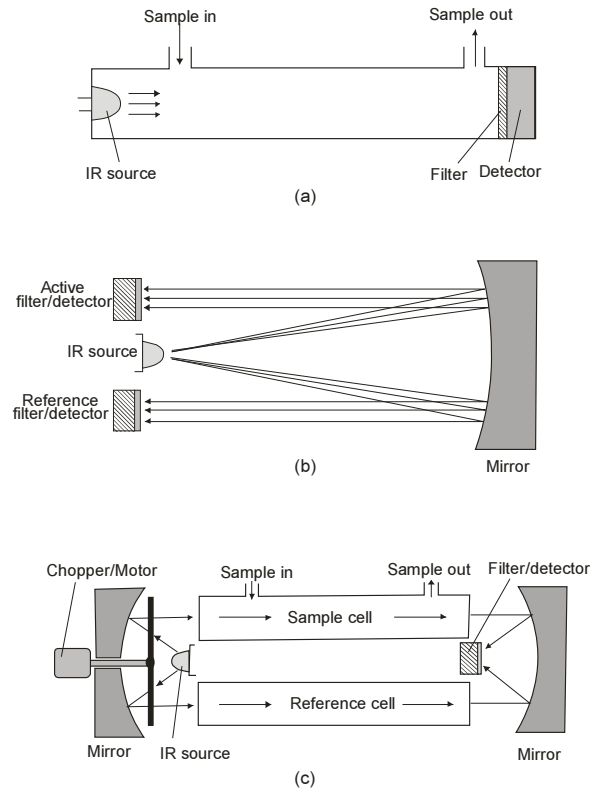


Fig. 47. Configurations of the gas analysers: (a) a basic gas detector layout, (b) a two-detector layout and (c) double beams with a chopper layout. Reproduced from [37].

In practice, in order to reduce false alarms and introduce a level of quantification, it is necessary to provide some calibration. According to the application and instrument manufacturer, this may take the form of a reference chamber containing a known concentration of the gas, or measurement of a reference wavelength just slightly outside the absorption band and/or dual matched detectors.

Figure 47(b) shows another popular design with a layout of two detectors. Modulated flashing IR sources are reflected back to the detectors. In this arrangement, the active detector

has a filter for the target gas, while the reference detector has a filter with a different wavelength. In such a way, the active detector is used to detect the target gas and the reference detector is used to ignore the target gas. In actual operation, the reference detector provides a base point value (or zero point) while the active detector is used to provide the signal. An advantage of this design is compensation of the changes that occur in the detector's sensitivity with time (for example, change in the intensity of the light source).

The design illustrated in figure 47(c) uses two tubes or cells. One is a reference cell that is filled with a pure target or reference gas, while the other is a sampling cell in which the sample gas passes through. Additionally, a chopper in the form of a disc is used, with a number of slots inside. As the chopper rotates, it alternately allows the light beam to pass through the sample and reference cells. The detector gets its base reading from the reference cell.

There are many light sources available, ranging from a regular incandescent light bulb to specially designated heating filaments and electronically generated sources. The latter sources are used to generate enough radiation at the wavelength of interest for the purpose of detecting the specific target gas. A heated wire filament, similar to that in a pen flashlight, is used in the 1–5  $\mu\text{m}$  spectral range for the detection of most hydrocarbons, carbon dioxide and carbon monoxide. Alternatives include glowbars (rods of silicon carbide) or coils, typically of nichrome alloy resistance wire with high emissivity in the MWIR region. Much recent research has concentrated on development of sources that are both more spectrally efficient and capable of more rapid modulation frequencies. The new sources can be categorized as thin incandescent membranes based on MEMS and technology, some of which have engineered high emissivity surfaces and light emitting diodes (LEDs) [36].

The selection of the optimum operating conditions for a gas analyzer is always a tradeoff between the required sensitivity and an operational system. In conventional absorption spectroscopy, using broadband incoherent radiation sources, the wavelength resolution is determined by the resolving power of the spectral analyzer or spectrometer. Laser absorption spectroscopy, on the other hand, uses coherent light sources, whose linewidths can be ultra-narrow and whose spectral densities can be made many orders of magnitude larger ( $\sim 10^9 \text{ W/cm}^2 \text{ MHz}$ ) than those of incoherent light sources. As it can be seen from figure 48, the whole spectral range from the visible to the infrared can be covered by semiconductor lasers of various compounds, which are mainly gallium arsenide, indium phosphite, antimonides and lead salts.

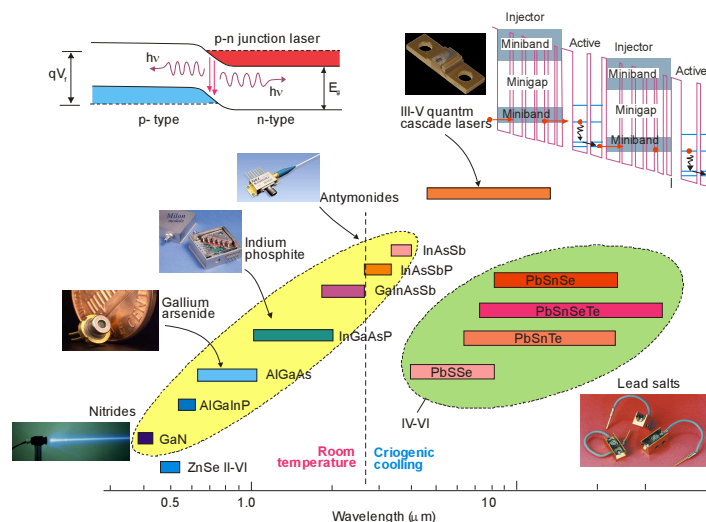


Fig. 48. Coverage of the spectral range from the visible to the infrared by tunable diode lasers of different material systems.

Up to the end of the 20th century, a drawback for industrial applications of gas analyzers based on semiconductor lasers was the lack of high-quality, high-power laser diodes for many spectral regions of interest. These lasers relied on direct band-to-band transitions in bulk material or analogous transition in type I quantum wells. Since the mid 1990s, lead salt and antimonide lasers have been facing competition from the quantum-cascade lasers (QCLs) [38] and type II quantum-well lasers (interband cascade lasers - ICLs) [39]. Quantum-cascade lasers operate on transitions within the conduction subbands of multiple quantum wells and have been pioneered by Bell Laboratories. Operation in IR region above the room temperature has been reported. These new types of laser are commercial/research available and they appear to offer the prospect of more robust construction and higher temperature operation than is possible with the materials that have been used up to this point. Trace-gas optical spectroscopic sensors using QCLs and ICLs are ultrasensitive and can detect molecular species at concentration levels from the percent level down to parts per trillion (ppt).

Today, tunable diode laser spectroscopy (TDLS) is a widely used technique for environmental monitoring, remote sensing, and process gas analytics. TDLS has rapidly become the most commonly used laser-based technique for quantitative measurements of species in gas phase. It is a highly selective, sensitive and versatile fast operation technique (up to MHz) for measuring trace species. The diode laser source is ideal for optical spectroscopy because of its narrow line width, tunability, stability, compactness, and ability to operate at the room temperature.

The basic TDLS measurement setup is fairly simple, as shown in figure 49 – it contains a laser diode at the right wavelength which is tunable, a gas cell and a detector. The exact wavelength of the laser can be tuned slightly over the absorption line from  $\nu_1$  to  $\nu_2$  by changing the laser temperature and/or the current. The laser light passes through the gas sample and the laser power transmitted through the sample is detected as a function of the laser wavelength. When the laser emission wavelength coincides with a resonant absorption in the molecule we see a sharp absorption signal. Direct absorption measurements have to resolve small changes  $\Delta I$  in a large signal offset  $I_0$ . The highest sensitivity is achieved at low gas pressure, when absorption lines are not substantially pressure broadened.

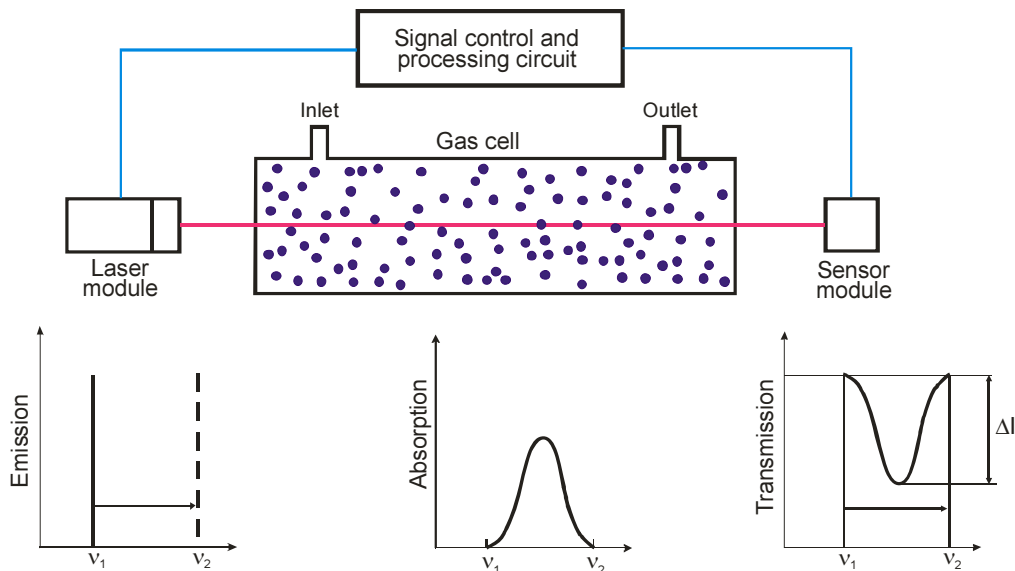


Fig. 49. Basic setup for laser spectroscopy.

To increase the signal-to-noise ratio (SNR) an additional noise suppression can be achieved by the application of modulation techniques. In modulation spectroscopy, the laser injection current is modulated at  $\omega_m$  while the laser wavelength is tuned repeatedly over the selected absorption line to accumulate the signal from the lock-in amplifier with a digital

signal averager (figure 50). This produces a derivative line profile with an amplitude proportional to the species concentration.

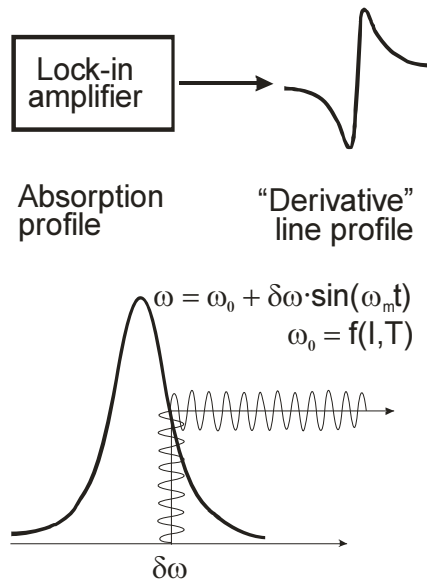


Fig. 50. Wavelength modulation spectroscopy.

The benefits of modulation spectroscopy are twofold: (i), offsets are eliminated (zero baseline technique) as it produces a derivative signal, directly proportional to the species concentration and, (ii), it allows narrowband detection of the signal at a frequency at which the laser noise is reduced.

To provide high sensitivity the long-path absorption cells,  $L$ , are required. This method is often used in open path measurement techniques such as remote sensing, where  $L$  are usually from tens of centimeters to several meters (see figure 51(a)).

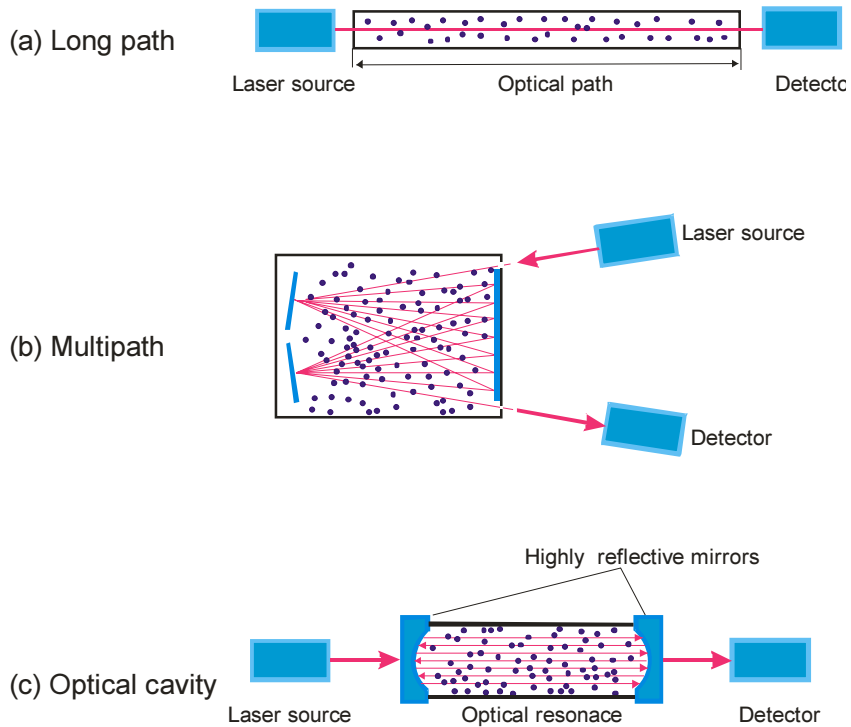


Fig. 51. Different approaches of gas cells. Reproduced from [40].

However, most of conventional trace-gas sensors have gas cells inside them. To increase their sensitivity and reduce the size of the apparatus the multipath cells are used (see figure 51(b)). The laser light enters the gas cell and is reflected many times by mirrors that are located at either end of the cell. In this way, we can obtain a long effective light path of tens to hundreds of meters with a gas cell whose actual length is less than 1 m.

Another method that uses an optical cavity is shown in figure 51(c). This method utilizes optical resonance with highly reflective mirrors and traps laser light in a cell. We can obtain a very long effective light path that exceeds several kilometers.

## 8. Conclusions

This chapter is about general IR engineering, technology, practices, and principles as they apply to modern infrared techniques. The information contained here is critical in the day-to-day life of engineering practitioners and those on the periphery of IR techniques. It serves rather as a guide for those wishing to “catch up” general information to the field, managers, students, and technicians. We miss the traditional development of equations and conclusions from first principles – they are presented in many other texts. Therefore, the chapter functions as a compilation of the state of the art, and provides background information for the reader devoted to infrared devices and techniques. It is concentrated on physical fundamentals of infrared radiation and practical instruments for military applications, metrology, astronomy, environmental monitoring, surveillance, commercial, and industrial uses.

## References

- [1] Herschel, W. (1800). Experiments on the refrangibility of the invisible rays of the Sun, *Phil. Trans. Roy. Soc. London* 90, 284.
- [2] Ross, W. (1994). *Introduction to Radiometry and Photometry*. Boston: Artech.
- [3] Hudson, R. D. (1969). *Infrared System Engineering*. New York: Wiley.
- [4] Rogalski, A. (2010). *Infrared Detectors*. Boca Raton: CRC Press.
- [5] <http://www.electronics-ca.com/infrared-detectors-market-report.html>
- [6] Couture, M. E. (2001). Challenges in IR optics, *Proc. SPIE* 4369, 649–661.
- [7] Harris, D. C. (1999). *Materials for Infrared Windows and Domes*. Bellingham: SPIE Optical Engineering Press.
- [8] Smith, W. J. (2000). *Modern Optical Engineering*. New York: McGraw-Hill.
- [9] Lloyd, J. M. (1975). *Thermal Imaging Systems*. New York: Plenum.
- [10] Kozlowski, L. J., Kosonocky, W. F. (1995). *Infrared detector arrays Handbook of Optics*, Chapter 23, ed M. Bass, E. W., Van Stryland, D. R., Williams, W. L., Wolfe. New York: McGraw-Hill.
- [11] Mooney, J. M., Shepherd, F. D., Ewing, W. S., Silverman, J. (1989). Responsivity nonuniformity limited performance of infrared staring cameras, *Opt. Eng.* 28, 1151–1161.
- [12] Chrzanowski, K. (2013). Review of night vision technology, *Opto-Electron. Rev.* 21, 153–182.
- [13] [http://www.hamamatsu.com/resources/pdf/etd/II\\_TII0004E02.pdf](http://www.hamamatsu.com/resources/pdf/etd/II_TII0004E02.pdf)
- [14] Cameron, A. S. (1990). The development of the combiner eyepiece night vision goggle, *Proc. SPIE* 1290, 16–19.
- [15] Csorba, I. P. (1985). *Image Tubes*, Indianapolis: Sams.
- [16] [https://customeronline.thalesgroup.com/sites/default/files/asset/document/hel\\_topowl\\_en.pdf](https://customeronline.thalesgroup.com/sites/default/files/asset/document/hel_topowl_en.pdf)
- [17] Miller, J. L. (1994). *Principles of Infrared Technology*. New York: Van Nostrand Reinhold.
- [18] STANAG No. 4349 *Measurement of the Minimum Resolvable Temperature Difference (MRTD) of Thermal Cameras*.

- [19] Campana, S. B. (1993). *The Infrared and Electro-Optical Systems Handbook*, vol 5, Passive Electro-Optical Systems, SPIE Optical Engineering Press Bellingham.
- [20] [http://www.ipac.caltech.edu/pdf/FIR-SMM\\_Crosscutting\\_Whitepaper.pdf](http://www.ipac.caltech.edu/pdf/FIR-SMM_Crosscutting_Whitepaper.pdf)
- [21] Chrzanowski, K. (2001). *Non-Contact Thermometry—Measurement Errors, Research and Development Treaties*, 7, Warsaw: SPIE Polish Chapter.
- [22] <http://www.landinst.com>
- [23] <http://www.fluke.com>
- [24] <http://www.vigo.com.pl>
- [25] <http://www.lumasense.com>
- [26] <http://www.abb.com>
- [27] [http://landsat.usgs.gov/band\\_designations\\_landsat\\_satellites.php](http://landsat.usgs.gov/band_designations_landsat_satellites.php)
- [28] [http://www.dlr.de/eoc/en/Portaldata/60/Resources/images/2\\_dfd\\_la/DFD-LA-AbbSpek\\_en\\_2048.jpg](http://www.dlr.de/eoc/en/Portaldata/60/Resources/images/2_dfd_la/DFD-LA-AbbSpek_en_2048.jpg)
- [29] <http://bioengineering/antiparticle?articled=1307622#r20>
- [30] Argall, P. S., Sica, R. J. (2003). Lidar (Laser Radar), in *The Optics Encyclopedia*, ed Th.G. Brown, K., Creath, H., Kogelnik, M. A., Kriss, J., Schmit, M. J., Weber. Berlin: Wiley-VCH.
- [31] [http://www.csc.noaa.gov/digitalcoast/\\_pdf/lidar101.pdf](http://www.csc.noaa.gov/digitalcoast/_pdf/lidar101.pdf)
- [32] <http://oceanservice.noaa.gov/facts/lidar.html>
- [33] Svanberg, S. (1990). Environmental monitoring using optical techniques, in *Applied Laser Spectroscopy*, 417–434, Demtröder, W., Inguscio, M. New York: Plenum.
- [34] Wolf, J. P., Kölsch, H. J., Rairoux, P., Wöste, L. (1990). Remote detection of atmospheric pollutants using differential absorption lidar techniques, in *Applied Laser Spectroscopy*, 435–467. Demtröder, W., Inguscio, M. New York: Plenum.
- [35] Luft, K. V. (1943). Über eine neue Methode der Registrierenden Gasanalyse mit Hilfe der Absorption Ultraroter Strahlen ohne Spektrale Zerlegu, *Z. Tech. Phys.* 24, 97–104.
- [36] Hodgkinson, J., Tatam, R. P. (2013). Optical gas sensing: a review, *Meas. Sci. Technol.* 24, 012004, 59.
- [37] Chou, J. (2000). *Hazardous Gas Monitors*, New York: McGraw-Hill.
- [38] Capasso, F., Gmachl, C., Paiella, R., Tredicucci, A., Hutchinson, A. L., Sivco, D. L., Baillargeon, J. N., Cho, A.Y. (2000). New frontiers in quantum cascade lasers and applications, *IEEE Selected Topics in Quantum Electronics* 6, 931–947.
- [39] Yang, R. Q., Bradshaw, J. L., Bruno, J. D., Pham, J. T., Wortman, D. E. (2002). Mid-infrared type II interband cascade lasers, *IEEE J. of Quant. Elect.* 38, 547–558.
- [40] Yoshimura, R., Kohtoku, M., Fujii, K., Sakamoto, T., Sakai, Y. (2014). Highly sensitive laser based trace-gas sensor technology and its application to stable isotope ratio analysis, *NTT Technical Review* 12(4), 1–6.